Report
P-18-08
January 2019

Forsmark – Laboratory tests for investigation of the influence of rock type, oxidation, and other factors in borehole breakouts

Boreholes KFM01A, KFM04A, KFM05A and KFM24

Thermal properties by TPS method and uniaxial compression and indirect tensile strength tests of intact rock

Lars Jacobsson
Johan Sjöström

SVENSK KÄRNBRÄNSLEHANTERING AB

SWEDISH NUCLEAR FUEL
AND WASTE MANAGEMENT CO

Box 3091, SE-169 03 Solna
Phone +46 8 459 84 00
skb.se

SVENSK KÄRNBRÄNSLEHANTERING

ISSN 1651-4416
SKB P-18-08
ID 1684535

January 2019
Updated 2020-10

Forsmark – Laboratory tests for investigation of the influence of rock type, oxidation, and other factors in borehole breakouts

Boreholes KFM01A, KFM04A, KFM05A and KFM24

Thermal properties by TPS method and uniaxial compression and indirect tensile strength tests of intact rock

Lars Jacobsson, Johan Sjöström
RISE Research Institutes of Sweden

Keywords: Thermal properties, Uniaxial compression test, Tensile strength test.

Update notice

The original report, dated January 2019, was found to contain both factual and editorial errors which have been corrected in this updated version. The corrected factual errors are presented below.

Updated 2020-10

Location	Original text	Corrected text
Page 3, Abstract, paragraph 4, line 2	2814	2722
Page 3, Abstract, paragraph 4, line 3	2768	2678
Page 4, Sammanfattning, paragraph 4, line 2	2814	2722
Page 4, Sammanfattning, paragraph 4, line 2	2768	2678
Page 16, Table 3-1, Core-specimen number 17-1, 17-2 and 17-3	Granite to granodiorite (101057)	Amphibolite (102017)
Page 17, Table 3-2, Identification KFM05A-90V-15	Granite to granodiorite (101057)	Amphibolite (102017)
Page 18, Table 3-3, Identification KFM05A-110-25, KFM05A-110-26 and KFM05A-110-27	Granite to granodiorite (101057)	Amphibolite (102017)
Page 29 and 31, Figure 6-1, 6-2 and 6-3	*Wrong symbol at 600 m depth*	*Figures updated with correct symbol at 600 m depth for Amphibolite*

Abstract

The density, thermal and mechanical properties were determined on water saturated specimens from boreholes KFM01A, KFM04A, KFM05A and KFM24 in the Forsmark site investigation area. The tests have been concentrated to sections where borehole breakouts have been observed. The rock types in the selected sections were amphibolite (102017), granite to granodiorite (101057) and skarn (108018). All specimens had a more or less foliated rock structure. The cores were sampled from a depth ranging between 308–929 m.

The specimens were water saturated using tap water and all subsequent measurements were conducted at this moisture condition. The density was determined on 41 specimens followed by measuring the thermal properties of 20 pairs of specimens. The thermal conductivity and diffusivity were measured and the volumetric heat capacity was calculated from the thermal conductivity and diffusivity. The testing ended with 35 indirect tensile tests yielding the indirect tensile strength and three uniaxial compression tests including the post-peak response yielded the Young's modulus, Poisson ratio and the uniaxial compressive strength.

Three specimens aimed for the indirect tensile tests had a major crack and fell apart after measuring the density and the mechanical properties were not tested.

Some variation of rock material along the short cores could be seen, which is reflected in the measured data. The density at a water saturated condition was 2 640–2 722 kg/m^3 for granite to granodiorite, 2 678–3 033 kg/m^3 for amphibolite and 2 787–2 920 kg/m^3 for skarn.

Thermal properties were measured at ambient temperature (22 °C) and under water saturated conditions. The determination of the thermal properties is based on a direct measurement method, the so called "Transient Plane Source Method" (TPS).

Thermal conductivity and thermal diffusivity at 22 °C were in the range of 1.6–3.5 W/(m, K) and 0.9–1.9 mm^2/s, respectively. The volumetric heat capacity, which was calculated from the thermal conductivity and diffusivity, ranged between 1.6 and 2.6 MJ/(m^3, K). Variations are most likely due to both depth and variations in rock type.

The indirect tensile tests were conducted such that every second specimen was tested with the diametrical compression along and every second across the foliation planes, with higher values for the indirect tensile strength on the specimens with loading across the foliation. The ratio between the strength measured on specimens with loading across over along the foliation was up to 1.6 for granodiorite and possible higher for the amphibolite. The strength variation in the amphibolite was large. The indirect tensile strength was 8.07–14.5 MPa for the granite to granodiorite, 1.18–16.2 MPa for amphibolite and 4.49–8.51 MPa for skarn.

Two of the uniaxial compression test specimens of amphibolite got a diagonal failure and the third had a spalling failure. The maximum axial compressive stress was 61.5 and 68.5 MPa for the specimens with a diagonal failure and 238.7 MPa for the specimen with a spalling failure. The Young's modulus for the same specimens was 61.6 and 57.5 GPa, respectively 91.0 GPa and the Poisson ratio 0.288 and 0.407, respectively 0.375.

Sammanfattning

Densiteten, termiska och mekaniska egenskaper har bestämts på vattenmättade prover from borrhål KFM01A, KFM04A, KFM05A och KFM24 i Forsmarks platsundersökningsområde. Provningarna har koncentrerats till avsnitt där s k ”borehole breakouts” har observerats. Bergarterna i de valda avsnitten är amfibolit (102017), granit till granodiorit (101057) och skarn (108018). Samtliga prover hade en mer eller mindre folierad bergstruktur. Proverna har tagits på djupnivåer mellan 308–929 m.

Proverna vattenmättades med kranvatten och alla efterföljande mätningar gjordes vid denna fukthalt. Densiteten mättes på samtliga 41 prover följt av mätning av de termiska egenskaperna på 20 par prover. Termisk konduktivitet och termisk diffusivitet mättes varefter den volumetriska värmekapaciteten beräknades. Provningen avslutades med 35 stycken indirekta test av draghållfastheten som gav den indirekta draghållfastheten och tre enaxiella kompressionsförsök inkluderat efterbrottsbeteende som gav värden på elasticitetsmodul, Poissons tal och enaxiell tryckhållfasthet.

Tre prover som var avsedda för indirekta dragförsök hade initialt en spricka och föll isär efter mätningen av densiteten och ingen mekanisk provning genomfördes.

En viss variation av bergmaterialet kunde ses på de korta kärnorna som visade sig i uppmätta data. Densiteten i ett vattenmättat tillstånd var 2 640–2 722 kg/m^3 hos granit till granodiorit, 2 678–3 033 kg/m^3 hos amfibolit och 2 787–2 920 kg/m^3 hos skarn.

Termisk konduktivitet och termisk diffusivitet har bestämts vid rumstemperatur (22 °C) och vattenmättnad. Mätningarna av egenskaperna utfördes med den direkta metoden “Transient Plane Source” (TPS).

Termisk konduktivitet och termisk diffusivitet vid 22 °C bestämdes till 1.6–3.5 W/(m, K) respektive 0.9–1.9 mm^2/s. Den volumetriska värmekapaciteten (produkten av densitet och specifk värmekapacitet), som beräknades från konduktivitet och diffusivitet, varierade mellan 1.6 and 2.6 MJ/(m^3, K). Variationerna beror antagligen både på djup och på variationer i materialtyp.

De indirekta dragförsöken utfördes så att vartannat prov belastades med diametral kompression längs med och vartannat tvärs foliationsplanen. Kvoten mellan styrkan mätt med belastning tvärs och längs med foliationen var upp till 1,6 för granit till granodiorit och möjligen högre för amfibolit. Styrkevariationen var stor hos amfibolit. Den indirekta draghållfastheten var 8,07–14,5 MPa hos granit till granodoiorit, 1,18–16,2 MPa hos amfibolit, och 4,49–8,52 MPa hos skarn.

Vid de enaxiella kompressionsförsöken fick två av amfibolitproverna ett diagonalt brott och det tredje ett spjälkningsbrott. Den högsta axialspänningen var 61,5 och 68,5 MPa hos proverna som hade ett diagonalt brott och 238,7 MPa hos provet med ett spjälkningsbrott. Elasticitetsmoduluen var 61,6 och 57.5 GPa respektive 91,0 GPa och Poisson’s tal var 0,288 och 0,407 respektive 0,375.

Contents

1 Introduction

This document reports performance and results of measurements of density, thermal properties, indirect tensile tests and uniaxial compression tests, with loading beyond the failure point into the post-failure regime, on water-saturated drill core specimens. The drill cores originate from the boreholes KFM01A, KFM04A, KFM05A and KFM24 which are located within the site investigation area in Forsmark, see map in Figure 1-1. The boreholes are conventionally drilled cored boreholes, with a length of c 550–1 000 m and are drilled with an inclination of 60–85 degrees relatively to the horizontal plane. The tests are concentrated to amphibolite (102017), granite to granodiorite (101057) and skarn (108018) where borehole breakouts were observed.

The tests were carried out in the material and rock mechanics laboratories at the Department of Safety at RISE Research Institutes of Sweden and at Swedish Cement and Concrete Research Institute (CBI) in Borås. CBI is a part of RISE.

SKB sent rock cores to RISE which arrived to Borås in July 2017 and were tested during August to October 2017. A planning of how to extract specimens was first conducted together with SKB and Geosigma. Cylindrical specimens were cut from the cores based on the plan. The end surfaces of the specimens were grinded in order to comply with the required shape tolerances. The specimens were water saturated and stored in water with a minimum of 7 days, up to testing. This yields a water saturation which is intended to resemble the in-situ moisture condition. All tests were carried out at this moisture condition. The density was first determined on each specimen followed by measurement of thermal properties and finally the mechanical tests were conducted.

The method description SKB MD 160.002e was followed for the water saturation and density measurements. The thermal properties, i.e. thermal conductivity and thermal diffusivity, have been determined by using the Transient Plane Source Method (TPS), Gustafsson (1991). The volumetric heat capacity can be calculated if the density is known. The method description SKB MD 191.001e was followed for the measurement of the thermal properties. The tests also comply to ISO 22007-2:2015 (ISO 2015) except that the specimens are not plastics. The method description SKB MD 190.004e was followed for the sampling and for the indirect tensile strength tests and the method description SKB MD 190.001e was followed for the uniaxial compression tests.

The rock material had a foliated structure in most of the specimens, which implies that both the thermal and mechanical properties are anisotropic. The foliation direction relative to the core axis differed between the specimens. The thermal measurements and uniaxial compression tests were carried out in the axial direction of the specimens. Hence, the properties were measured relative the foliation angles given by the foliation orientation in the specimens. At the indirect tensile tests the direction of loading the direction of loading could be chosen. A line was drawn on each specimen showing the direction of loading. The loading directions were evenly distributed with half of the specimens loaded apparently parallel to the foliation and the other half of the specimens apparently perpendicular to the foliation, by just determining the foliation orientation by looking on the circular cross section surfaces. Note that a true loading parallel or perpendicular to the foliation would require that the foliation direction has to be parallel to the specimen axis, which is not the case here.

The thermal conductivity is assumed isotropic despite the foliated structure according to discussions prior to testing. This will yield a result in between the conductivity in axial and through-plane direction.

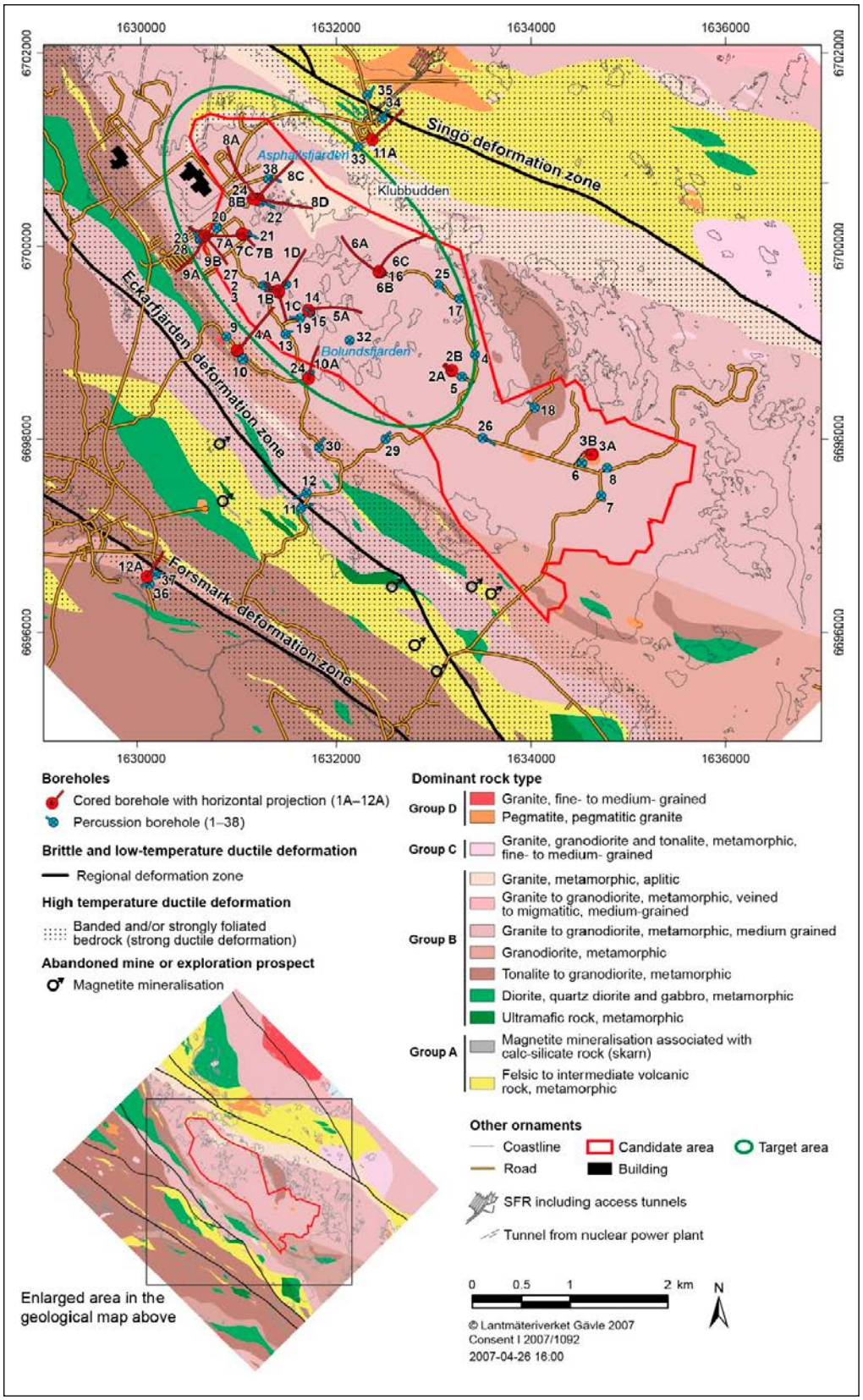

Figure 1-1. *Geological map showing the location of all boreholes drilled up to April 2007 within or close to the Forsmark candidate area. The projection of each borehole on the horizontal plane at top of casing is also shown in the figure.*

The controlling documents for the activity are listed in Table 1-1. Both Activity Plan and Method Descriptions are SKB's internal controlling documents, whereas the Quality Plan referred to in the table is an RISE internal controlling document.

Table 1-1. Controlling documents for performance of the activity.

Activity plan	**Number**	**Version**
Bergmekaniska och termiska laboratorietester med prover från Forsmark	AP SFK-17-025	1.0
Method descriptions	**Number**	**Version**
Determining density and porosity of intact rock	SKB MD 160.002e	3.0
Uniaxial compression test for intact rock	SKB MD 190.001e	4.0
Indirect test of tensile strength	SKB MD 190.004e	3.0
Determining thermal conductivity and thermal capacity	SKB MD 191.001e	3.0
Quality plan		
Activity specific quality plan	RISE document	

2 Objective

A number of test batches have been conducted earlier on drill cores from the boreholes KFM01A to KFM09A within the site investigation program in Forsmark. The material from the first test batches has now been processed by SKB's modelers. Some conclusions can be drawn from the processed data of the test results. Early on in the investigations, borehole breakouts were found in the boreholes. The sampling and laboratory determinations of the mechanical and thermal properties were selected according to the rock types and test methods that were judged to be most prioritized with respect to borehole breakouts after discussion with the modelers for the rock mechanical and thermal modelling.

The tests were concentrated to the boreholes KFM01A, KFM04A, KFM05A and KFM24 and to the rock type amphibolite (102017) as well as granite to granodiorite (101057) where borehole breakouts and micro fallouts were observed. The objective is to increase the understanding of the mechanisms behind spalling in an early and a late stage in boreholes as well as effects from rock type, oxidation, etc. An investigation area within skarn (108018) was also judged to be of interest for this investigation since a strong indication of borehole breakouts was found. Another goal is to increase the knowledge of the mechanical properties of amphibolite, i.e. completing the Sicada database regarding the amphibolite.

The evaluation of the test results and assessment of mechanisms behind borehole breakouts are not included in this work and are reported elsewhere.

3 Specimens

Each specimen is subjected to three measurements, density, thermal and mechanical. To distinguish the investigations and to cohere with the method descriptions, different labelling is introduced for the specimens when thermal and mechanical tests are conducted even if it is the same physical specimens.

3.1 Extraction plan

A total of 12 core parts were selected for this investigation, four parts from KFM01A, four parts from KFM04A, two parts from KFM05A and two parts from KFM24. A plan for how to extract specimens for the different investigations was made together with SKB and Geosigma. The markings of how to extract the specimens from the individual cores including observations of defects are shown in Figures 3-1 to 3-4. Three specimens, denoted 1b in Figures 3-2 and 3-4, were extracted on order to make a pair in order to be able to measure the thermal properties of the uniaxial compression test specimens. The extra specimens have the same size as the specimens for the indirect tensile tests and were therefore also designated to mechanical testing.

The specimens were marked with arrows to keep track of the orientation on the core. The rock type characterisation was made according to Stråhle (2001) using the SKB mapping system (Boremap). The labelling and position in the borehole (adj secup and adj seclow) and test designation for the individual specimens are shown in Table 3-1.

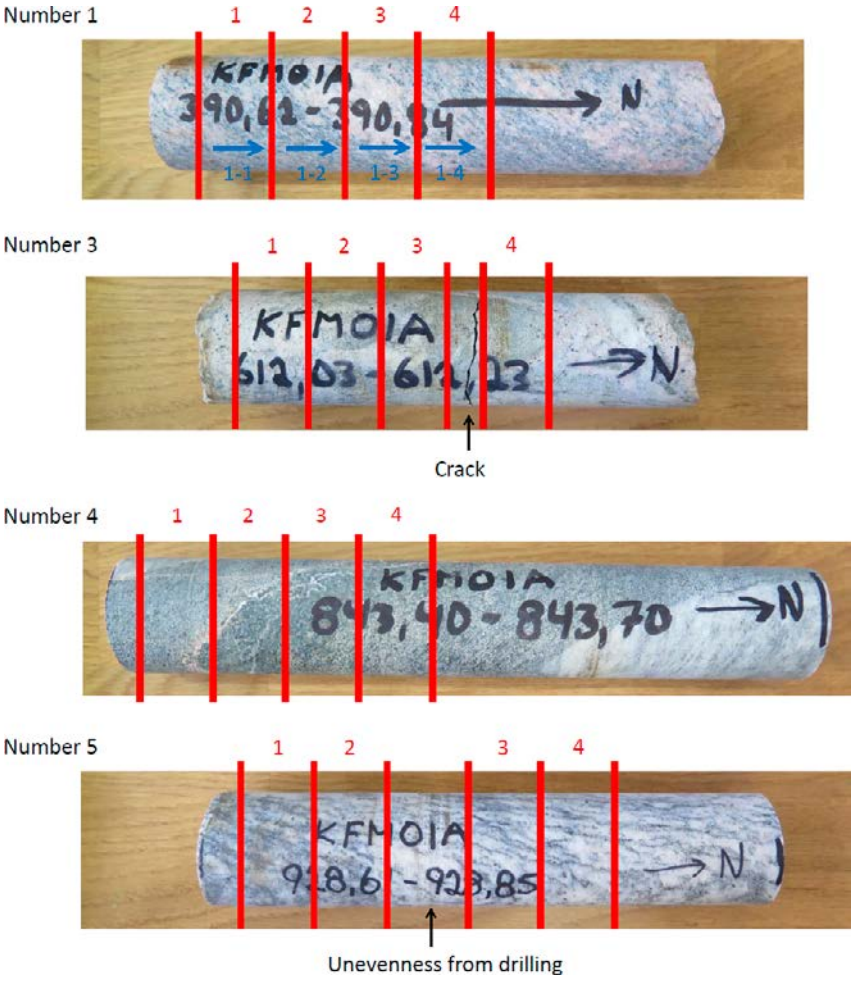

Figure 3-1. *Layout for cutting the specimens from KFM01A, cores 1, 3, 4 and 5.*

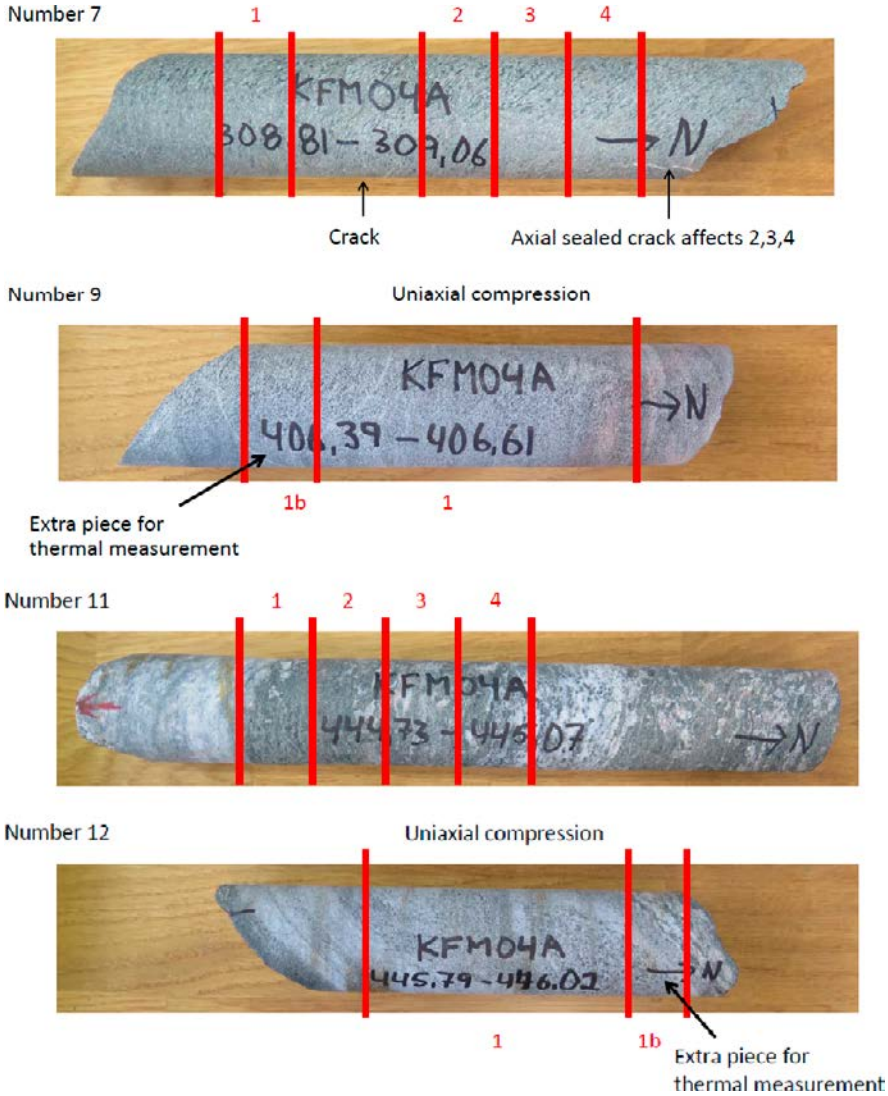

Figure 3-2. *Layout for cutting the specimens from KFM04A, cores 7, 9, 11 and 12.*

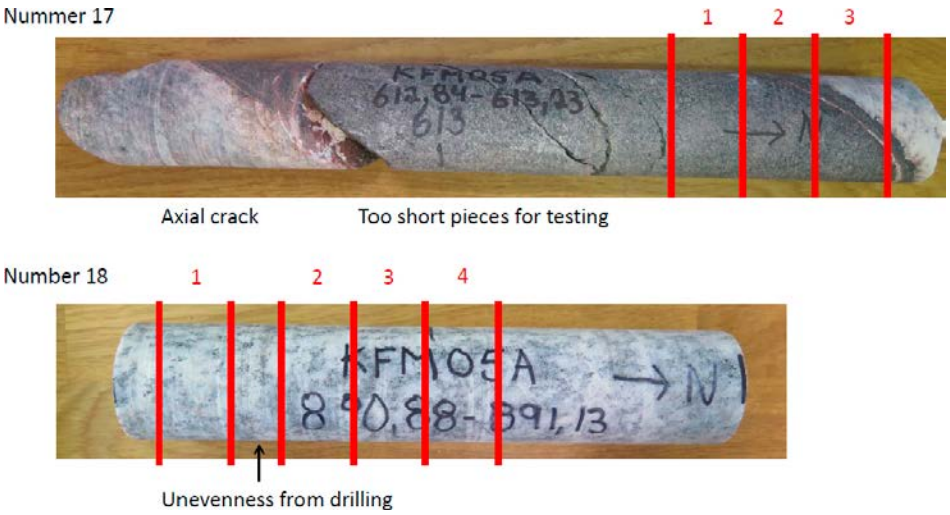

Figure 3-3. *Layout for cutting the specimens from KFM05A, cores 17 and 18.*

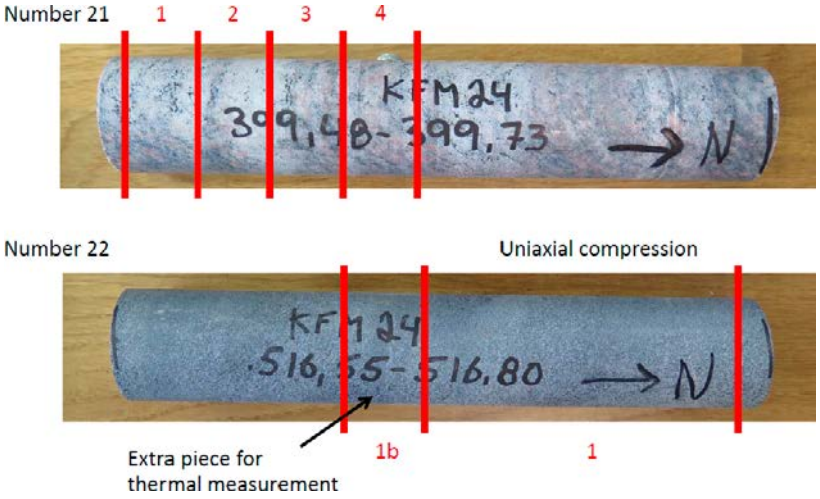

Figure 3-4. *Layout for cutting the specimens from KFM24, cores 21 and 22.*

Table 3-1. Core and specimen identification, sampling level (borehole length) and rock type for all specimens (based on the Boremap overview mapping).

Core-specimen number	Borehole	Adj Secup (m)	Adj Seclow (m)	Mechanical Test	Rock type/occurrence
1-1	KFM01A	390.63	390.66	BR	Granite to granodiorite (101057)
1-2	KFM01A	390.66	390.69	BR	Granite to granodiorite (101057)
1-3	KFM01A	390.69	390.72	BR	Granite to granodiorite (101057)
1-4	KFM01A	390.72	390.75	BR	Granite to granodiorite (101057)
3-1	KFM01A	612.04	612.07	BR	Skarn (108018)
3-2	KFM01A	612.07	612.10	BR	Skarn (108018)
3-3	KFM01A	612.10	612.13	BR	Skarn (108018)
3-4	KFM01A	612.15	612.18	BR	Skarn (108018)
4-1	KFM01A	843.41	843.44	BR	Amphibolite (102017)
4-2	KFM01A	843.44	843.47	BR	Amphibolite (102017)
4-3	KFM01A	843.47	843.50	BR	Amphibolite (102017)
4-4	KFM01A	843.50	843.53	BR	Amphibolite (102017)
5-1	KFM01A	928.62	928.65	BR	Granite to granodiorite (101057)
5-2	KFM01A	928.65	928.68	BR	Granite to granodiorite (101057)
5-3	KFM01A	928.72	928.75	BR	Granite to granodiorite (101057)
5-4	KFM01A	928.75	928.78	BR	Granite to granodiorite (101057)
7-1	KFM04A	308.85	308.88	BR	Amphibolite (102017)
7-2	KFM04A	308.95	308.98	BR	Amphibolite (102017)
7-3	KFM04A	309.98	309.01	BR	Amphibolite (102017)
7-4	KFM04A	309.01	309.04	BR	Amphibolite (102017)
9-1b	KFM04A	406.43	406.46	BR	Amphibolite (102017)
9-1	KFM04A	406.46	406.59	UCS	Amphibolite (102017)
11-1	KFM04A	444.76	444.79	BR	Amphibolite (102017)
11-2	KFM04A	444.79	444.82	BR	Amphibolite (102017)
11-3	KFM04A	444.82	444.85	BR	Amphibolite (102017)
11-4	KFM04A	444.85	444.88	BR	Amphibolite (102017)
12-1	KFM04A	445.84	445.97	UCS	Amphibolite (102017)
12-1b	KFM04A	445.97	446.00	BR	Amphibolite (102017)
17-1	KFM05A	613.11	613.14	BR	Amphibolite (102017)
17-2	KFM05A	613.14	613.17	BR	Amphibolite (102017)
17-3	KFM05A	613.17	613.20	BR	Amphibolite (102017)
18-1	KFM05A	890.89	890.92	BR	Granite to granodiorite (101057)
18-2	KFM05A	890.93	890.96	BR	Granite to granodiorite (101057)
18-3	KFM05A	890.96	890.99	BR	Granite to granodiorite (101057)
18-4	KFM05A	890.99	891.02	BR	Granite to granodiorite (101057)
21-1	KFM24	399.48	399.51	BR	Granite to granodiorite (101057)
21-2	KFM24	399.51	399.54	BR	Granite to granodiorite (101057)
21-3	KFM24	399.54	399.57	BR	Granite to granodiorite (101057)
21-4	KFM24	399.57	399.60	BR	Granite to granodiorite (101057)
22-1b	KFM24	516.64	516.67	BR	Amphibolite (102017)
22-1	KFM24	516.67	516.80	UCS	Amphibolite (102017)

Explanation to table: BR = Indirect tensile test, UCS uniaxial compression test.

3.2 Specimens for measuring thermal properties

The measurements of thermal properties are made with a thin sensor that is placed between two pieces of rock cores. Two of the extracted specimens are needed for one thermal measurement. Table 3-2 specifies the specimen interfaces where measurements have been conducted. Thus, KFM01A-90V-01 is the interface between two specimens where the sensor is placed. The upper and lower distance where the properties are probed denotes the distances within which the actual heat wave penetrates and not the physical distance of the specimens.

Table 3-2. Specimen interfaces used for measurements of thermal properties.

Identification	Adj Secup (m)	Adj Seclow (m)	Rock type/occurrence	Core numbers and specimens in Figure 3-1 to 3-4.
KFM01A-90V-01	390.65	390.67	Granite to granodiorite (101057)	Core 1-1 and core 1-2
KFM01A-90V-02	390.71	390.73	Granite to granodiorite (101057)	1-3 and 1-4
KFM01A-90V-03	612.06	612.09	Skarn (108018)	3-1 and 3-2
KFM01A-90V-04	612.12	612.16	Skarn (108018)	3-3 and 3-4
KFM01A-90V-05	843.43	843.45	Amphibolite (102017)	4-1 and 4-2
KFM01A-90V-06	843.49	843.51	Amphibolite (102017)	4-3 and 4-4
KFM01A-90V-07	928.64	928.66	Granite to granodiorite (101057)	5-1 and 5-2
KFM01A-90V-08	928.74	928.76	Granite to granodiorite (101057)	5-3 and 5-4
KFM04A-90V-09	308.87	308.96	Amphibolite (102017)	7-1 and 7-2
KFM04A-90V-10	309.00	309.02	Amphibolite (102017)	7-3 and 7-4
KFM04A-90V-11	406.45	406.47	Amphibolite (102017)	9-1 and 9-1b
KFM04A-90V-12	444.78	444.80	Amphibolite (102017)	11-1 and 11-2
KFM04A-90V-13	444.84	444.86	Amphibolite (102017)	11-3 and 11-4
KFM04A-90V-14	445.96	445.98	Amphibolite (102017)	12-1 and 12-1b
KFM05A-90V-15	613.13	613.15	Amphibolite (102017)	17-2 and 17-3
KFM05A-90V-16	890.91	890.94	Granite to granodiorite (101057)	18-1 and 18-2
KFM05A-90V-17	890.98	891.00	Granite to granodiorite (101057)	18-3 and 18-4
KFM24-90V-18	399.50	399.52	Granite to granodiorite (101057)	21-1 and 21-2
KFM24-90V-19	399.56	399.58	Granite to granodiorite (101057)	21-3 and 21-4
KFM24-90V-20	516.66	516.68	Amphibolite (102017)	22-1 and 22-1b

3.3 Specimens for indirect tensile tests

A list of 38 specimens for the indirect tensile tests is shown in Table 3-3.

Table 3-3. Specimen identification, sampling level (borehole length) and rock type for all specimens (based on the Boremap overview mapping).

Identification	Adj Secup (m)	Adj Seclow (m)	Rock type/occurrence
KFM01A-110-01	390.63	390.66	Granite to granodiorite (101057)
KFM01A-110-02	390.66	390.69	Granite to granodiorite (101057)
KFM01A-110-03	390.69	390.72	Granite to granodiorite (101057)
KFM01A-110-04	390.72	390.75	Granite to granodiorite (101057)
KFM01A-110-05	612.04	612.07	Skarn (108018)
KFM01A-110-06	612.07	612.10	Skarn (108018)
KFM01A-110-07	612.10	612.13	Skarn (108018)
KFM01A-110-08	612.15	612.18	Skarn (108018)
KFM01A-110-09	843.41	843.44	Amphibolite (102017)
KFM01A-110-10	843.44	843.47	Amphibolite (102017)
KFM01A-110-11	843.47	843.50	Amphibolite (102017)
KFM01A-110-12	843.50	843.53	Amphibolite (102017)
KFM01A-110-13	928.62	928.65	Granite to granodiorite (101057)
KFM01A-110-14	928.65	928.68	Granite to granodiorite (101057)
KFM01A-110-15	928.72	928.75	Granite to granodiorite (101057)
KFM01A-110-16	928.75	928.78	Granite to granodiorite (101057)
KFM04A-110-17	308.85	308.88	Amphibolite (102017)
KFM04A-110-18	308.95	308.98	Amphibolite (102017)
KFM04A-110-19	309.98	309.01	Amphibolite (102017)
KFM04A-110-20	309.01	309.04	Amphibolite (102017)
KFM04A-110-1b	406.43	406.46	Amphibolite (102017)
KFM04A-110-21	444.76	444.79	Amphibolite (102017)
KFM04A-110-22	444.79	444.82	Amphibolite (102017)
KFM04A-110-23	444.82	444.85	Amphibolite (102017)
KFM04A-110-24	444.85	444.88	Amphibolite (102017)
KFM04A-110-2b	445.97	446.00	Amphibolite (102017)
KFM05A-110-25	613.11	613.14	Amphibolite (102017)
KFM05A-110-26	613.14	613.17	Amphibolite (102017)
KFM05A-110-27	613.17	613.20	Amphibolite (102017)
KFM05A-110-28	890.89	890.92	Granite to granodiorite (101057)
KFM05A-110-29	890.93	890.96	Granite to granodiorite (101057)
KFM05A-110-30	890.96	890.99	Granite to granodiorite (101057)
KFM05A-110-31	890.99	891.02	Granite to granodiorite (101057)
KFM24-110-32	399.48	399.51	Granite to granodiorite (101057)
KFM24-110-33	399.51	399.54	Granite to granodiorite (101057)
KFM24-110-34	399.54	399.57	Granite to granodiorite (101057)
KFM24-110-35	399.57	399.60	Granite to granodiorite (101057)
KFM24-110-3b	516.64	516.67	Amphibolite (102017)

3.4 Specimens for uniaxial compression tests

A list of three specimens for the uniaxial compression tests is shown in Table 3-4.

Table 3-4. Specimen identification, sampling level (borehole length) and rock type for all specimens (based on the Boremap overview mapping).

Identification	Adj Secup (m)	Adj Seclow (m)	Rock type/occurrence
KFM04A 113-1	406.46	406.59	Amphibolite (102017)
KFM04A 113-2	445.84	445.97	Amphibolite (102017)
KFM24A 113-3	516.67	516.80	Amphibolite (102017)

4 Equipment

4.1 Specimen preparation

A circular saw with a diamond blade was used to cut the specimens to their final lengths. The surfaces were then grinded after cutting in a grinding machine in order to achieve a high-quality surface for the thermal measurements and axial loading that complies with the required tolerances. The measurements of the specimen dimensions were made with a sliding calliper. Furthermore, the tolerances were checked by means of a dial indicator and a stone face plate. The specimen preparation is carried out in accordance with ASTM (2001).

4.2 Water saturation and density measurement

The following equipment was used for the density and porosity determinations:

- Scale for weight measurement after water saturation (scale routinely checked with reference weight). Measurement accuracy ± 0.002 g.
- Scale for weight measurement after water saturation in surface dry condition (scale routinely checked with reference weight). Measurement accuracy ± 0.02 g.

4.3 Transient plane source

Technical devices for determination of the thermal properties in question were:

- Kapton insulated sensor 5501, with a radius of 6.4 mm. The sensor 5501 fulfils the recommended relation between sensor radius and sample geometry of the samples in ISO 22007-2.
- TPS-apparatus, TPS 2500s, see Figure 4-1 as well as the software Hotdisk Thermal Constants Analyser version 7.3.
- Stainless Sample holder and plastic bags around the specimen.

Function control of TPS instrumentation was performed according to BRk-QB-M26-02 (SP quality document), see Appendix A, as well as to the accredited standard ISO 22007-2:2015 (ISO 2015).

The experimental set-up is shown in Figure 4-2.

Figure 4-1. *TPS-apparatus TPS 2500s with sensor switch.*

Figure 4-2. *Specimens mounted in stainless sample holder (left), and sample holder with mounted specimens wrapped in plastic (right).*

4.4 Indirect tensile strength test

The mechanical testing was carried out in a load frame where the crossbar is mechanically driven by screws and has a maximum load capacity of 100 kN in compression. The axial compressive load was measured by an external 100 kN load cell. The uncertainty of the load measurement is less than 1 %. The frame was equipped with a pair of curved bearing blocks, radius 39 mm and width 29 mm, with pins for guiding the vertical deformation, see Figure 4-3. The top platen includes a spherical seating in order to have a fully centred loading position. The specimens were photographed with a 12.1 Mega pixel digital camera at highest resolution and the photographs were stored in a jpeg-format.

4.5 Uniaxial compression test

The mechanical tests were carried out in a servo controlled testing machine specially designed for rock tests, see Figure 4-4. The system consists of a load frame, a hydraulic pump unit, a controller unit and various sensors. The communication with the controller unit is accomplished by means of special testing software run on a PC connected to the controller. The load frame is characterized by a high stiffness and is supplied with a fast responding actuator, cf. the ISRM suggested method (ISRM 1999).

Figure 4-3. *Test-set up for the indirect tensile strength test. The load cell is visible in the top and the curved bearing blocks are seen below that.*

Figure 4-4. *Rock testing system. From left: Digital controller unit, pressure cabinet (used for triaxial tests) and load frame. The PC with the test software (not shown in the picture) is placed on the left hand side of the controller unit.*

The stiffness of the various components of the loading chain in the load frame has been optimized in order to obtain a high total stiffness. This includes the load frame, load cell, load platens and piston, as well as having a minimum amount of hydraulic oil in the cylinder. Furthermore, the sensors, the controller and the servo valve are rapidly responding components. The axial load is determined using a load cell, which has a maximum capacity of 1.5 MN. The uncertainty of the load measurement is less than 1 %.

The axial and circumferential (radial) deformations of the rock specimens were measured. The rock deformation measurement systems are based on miniature LVDTs with a measurement range of ± 2.5 mm. The relative error for the LVDTs is less than 0.6 % within a 1 mm range for the axial deformation measurements and less than 1.3 % within a 3 mm range for the circumferential deformation measurement. The LVDTs have been calibrated by means of a micrometer.

Two independent systems were used for the axial deformation measurement in order to obtain two comparative results. The first system (S1), see Figure 4-5, comprises two aluminium rings attached on the specimen, placed at ¼ and ¾ of the specimen height. Two LVDTs mounted on the rings are used to measure the distance change between the rings on opposite sides of the specimen. As to the attachment, two rubber bands made of a thin rubber hose with a total thickness of 1 mm thickness are first mounted on the specimen right under where the two rings are to be positioned. The rings are supplied with three adjustable spring-loaded screws, each with a rounded tip pointing on the specimen with 120 degrees division. The screw tips are thus pressing on the rubber band, when the rings are mounted. The second system (S2), see Figure 4-5, consists of two aluminium plates clamped around the circular loading platens of steel on top and on bottom of the specimen. Two LVDTs, mounted on the plates, measure the distance change between these plates at opposite sides of the specimen at corresponding positions as for the first measurement system (S1).

The radial deformation was obtained by using a chain mounted around the specimen at mid-height, see Figure 4-5 and Appendix 1. The change of the chain-opening gap was measured by means of one LVDT and the circumferential, and thereby also the radial deformation could be obtained. See Appendix 1.

The specimens were photographed with a 12.1 Mega pixel digital camera at highest resolution and the photographs were stored in a jpeg-format.

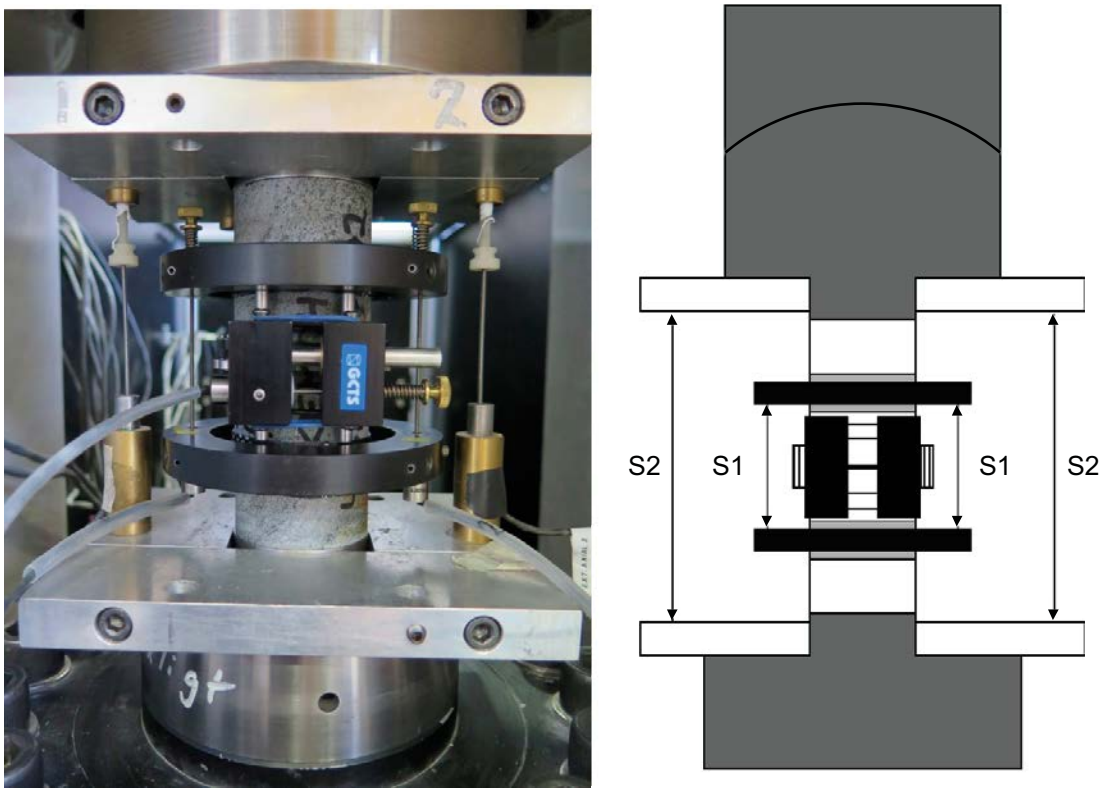

Figure 4-5. *Left: Specimen inserted between the loading platens. The two separate axial deformation measurement devices can be seen: system (S1) that measures the local axial deformation (rings), and system (S2) that measures the deformation between the aluminium plates (total deformation). Right: Principal sketch showing the two systems used for the axial deformation measurements.*

5 Execution

The specimens were going through following activities which are described in Section 5-1 to 5-6:

1. Cut and grind the specimens.
2. Take photographs of the specimens after the preparation.
3. Water saturation of the specimens for minimum 7 days.
4. Measure the wet density at a water saturated condition.
5. Measure the thermal properties at a water saturated condition.
6. Measure the mechanical properties at a water saturated condition.
7. Take photographs of the specimens after the mechanical tests.

5.1 Specimen preparation

The steps for the specimen preparation are shown in Table 5-1.

Table 5-1. Activities during the specimen preparation.

Step	Activity
1	The drill cores were marked where the specimens are to be taken.
2	The specimens were cut to the specified length according to markings and the cutting surfaces were grinded.
3	The tolerances were checked: parallel and perpendicular end surfaces, smooth and straight circumferential surface.
4	The diameter and height were measured three times each. The respective mean value determines the dimensions that are reported.

5.2 Water saturation and density measurement

The water saturation and determination of the density of the wet specimens were made in accordance with the method description SKB MD 160.002e (SKB internal controlling document). This includes determination of density in accordance to ISRM (1979) and water saturation by EN 13755 (CEN 2008).

The density of the water at the time for the measurements was 998 kg/m^3. The execution procedure followed the prescription in SKB MD 160.002e, see Table 5-2.

Table 5-2. Activities during the water saturation and density measurements.

Step	Activity
1	The specimens were water saturated using tap water in normal air pressure for at least seven days.
2	The specimens were weighed in tap water. The temperature of the water was measured and the water density was determined from a table.
3	The specimens were surface dried with a towel and weighed.
4	The density at a water saturated condition was determined.

5.3 Transient plane source

5.3.1 Principle of Transient Plane Source

The principle of the TPS-method is to install a sensor consisting of a thin Nickel double spiral, embedded in an insulation material, between two rock samples. During the measurement the sensor works both as a heat emitter (a constant electrical power is developed during a certain time) and

a heat receptor (the temperature increase of the sensor is measured through the resistivity of the Nickel due to the strong temperature dependence for the resistivity of Nickel). The input data and results of the direct measurement are registered and analysed by the same software and electronics that govern the measurement. The first part of the heating period is ignored to allow for boundary effects in the sensor/specimen interface to vanish. The last part can sometimes also be ignored to ensure that the heat wave do not exceed the diameter of the sensor, according to the measurement standard. The transient temperature evolution on the sensor, ΔT_s, is fitted to the equation of temperature increase of a sensor in a homogeneous, isotropic and semi-infinite material.

$$\Delta T_s(\tau) = P_0\left(\pi^{3/2} r k\right)^{-1} D(\tau),$$

where P_0 is power output of probe, r is the radius of the sensor, k is the thermal conductivity of the material, $\tau = (t/\theta)^{1/2}$, t is time, $\theta = r^2/\alpha$, α is the thermal diffusivity, and $D(\tau)$ is a dimensionless time function defined as:

$$D(\tau) = [m(m+1)]^{-2} \int_0^{\tau} \sigma^{-2} \left[\sum_{i=1}^{m} i \sum_{j=2}^{m} j \exp\left(\frac{-(i^2 + j^2)}{4m^2\sigma^2} \right) I_0\left(\frac{ij}{2m^2\sigma^2} \right) \right] d\sigma$$

where m is number of rings on the sensor spiral, σ is the integration variable and $I_0(x)$ is a modified Bessel function. Thus, there are only two fit parameters in the equation, the thermal conductivity – k, and the thermal diffusivity – α.

The volumetric heat capacity ρc_p, where ρ is the density and c_p is the specific heat capacity is obtained from the ratio between the thermal conductivity and diffusivity:

$$\rho c_p = k/\alpha$$

5.3.2 Test procedure

Determination of thermal properties conductivity and diffusivity was made in compliance with SKB's method description SKB MD 191.001 (SKB internal controlling document) and ISO 22007-2:2015 (ISO 2015) for Determination of thermal conductivity and thermal diffusivity at RISE Safety Fire Research. Fredrik Kahl and Johan Sjöström at RISE Safety conducted the thermal property measurements and preparation pertinent sections of the report.

The thermal properties of the water-saturated specimens were measured in ambient air (22 °C). In order to remain water saturation and obtain desired temperature, the specimens and the sensor were kept in a plastic bag during the measurements, see Figure 4-2.

Each pair of specimens was measured at least five times. The time lag between two repeated measurements was 50 minutes and every measurement was 40 s long. During the transient heating 200 data points of temperature increase is registered. Not all of them are used in the analysis as explained above. The result of each measurement was evaluated separately. The average value of all measurements for each specimen was calculated and presented here.

Measured raw data were saved and the analysis is saved for each measurement as Excel files. These files were stored on the hard disc of the measurement computer and sent to the project folder at the RISE network. Further calculations of mean values and standard deviations were performed in the same catalogue.

5.4 Indirect tensile strength test

The specimens had been stored more than 19 days in water when the indirect tensile strength was determined.

An auto-calibration of the load frame was run prior to the mechanical test in order to check the system. Further, an individual check-list was filled in and checked for every specimen during all the steps in the execution.

The diameter and thickness were entered into the test software which computed the indirect tensile strength together with the mean value and standard deviation for the whole test series. The results were then exported as text-files and stored in a file server on the RISE computer network

A list of the activities conducted during the indirect tensile strength tests is shown in Table 5-3.

Table 5-3. Activities during the indirect tensile strength tests.

Step	Activity
1	The geometrical tolerances were checked: parallel and perpendicular surfaces, smooth and straight circumferential surface.
2	The diameter and thickness were measured three times each. The respective mean value determines the dimensions that are reported.
3	The direction of compressive loading was marked as a line on one of the plane surfaces with a marker pen.
4	The specimens were then put into water and stored in water for minimum 7 days. The weight of water together with one specimen was determined. The specimen was taken out from the water and the weight of the water and rock specimen was determined separately, and by using the known density of the water, the wet density could be computed. This procedure was repeated for each specimen.
5	The wet specimens were inserted into the loading device one by one, with the correct orientation given by the marked line. The strain gauges were connected to the sampling device and the signals were checked. The specimens were loaded up to failure during deformation control. The displacement rate was set to 0.3 mm/min during loading. The maximum compressive load, which also defines the failure load, was registered

5.5 Uniaxial compression tests

5.5.1 Test procedure

The specimens had been stored more than 40 days in water when the uniaxial compression tests were carried out. The functionality of the testing system was checked before starting the tests.

An overview of the activities during the mechanical testing is shown in the step-by step description in Table 5-4.

Table 5-4. Activities during the uniaxial compression tests.

Step	Activity
1	Digital photos were taken on each specimen before the mechanical testing.
2	Devices for measuring axial and circumferential deformations were attached to the specimen.
3	The specimen was put in place and centred between the frame loading platens.
4	The core on each LVDT was adjusted by means of a set screw to the right initial position. This was done so that the optimal range of the LVDTs can be used for the deformation measurement.
5	The frame piston was brought down into contact with the specimen with a force corresponding to 1.0 MPa axial stress.
6	A load cycle with loading up to 5 MPa and unloading to 1.0 MPa was conducted in order to settle possible contact gaps in the spherical seat in the piston and between the rock specimen and the loading platens.
7	The centring was checked again.
8	The deformation measurement channels were zeroed in the test software.
9	The loading was started and the initial loading rate was set to a radial strain rate of -0.025 %/min. The loading rate was increased after reaching the post-failure region. This was done in order to prevent the total time for the test to become too long.
10	The test was stopped either manually when the test had proceeded long enough to reveal the post-failure behaviour, or after severe cracking had occurred and it was judged that very little residual axial loading capacity was left in the specimen.
11	Digital photos were taken on each specimen after the mechanical testing.

5.5.2 Analyses and interpretation

As to the definition of the different results parameters we begin with the axial stress σ_a, which is defined as

$$\sigma_a = \frac{F}{A}$$

where F is the axial force acting on the specimen, and A is the specimen cross section area. The peak value of the axial stress during a test is representing the uniaxial compressive strength σ_c in the results presentation.

The average value of the two axial displacement measurements on opposite sides of the specimen is used for the axial strain calculation, cf. Figure 4-5. In the first measurement system (S1), the recorded deformation represents a local axial deformation δ_{local} between the points at ¼ and ¾ height. A local axial strain is defined as

$$\varepsilon_{a,local} = \delta_{local}/L_{local}$$

where L_{local} is the centre to centre distance between the rings before loading.

In the second measurement system (S2), the recorded displacement corresponds to a total deformation that, in addition to total rock deformation, also contains the local deformations that occur in the contact between the rock and the loading platens, and further it also contains the deformation of the steel loading platens at each side of the specimen ends. The average value of the two total deformation measurements on opposite sides of the specimen is defined as the total deformation δ_{total}. An axial strain based on the total of the deformation is defined as

$$\varepsilon_{a,total} = \delta_{total}/L_{total}$$

where L_{total} is the height of the rock specimen.

The radial deformation is measured by means of a chain mounted around the specimen at mid-height, cf. Figure 4-5. The change of chain opening gap is measured by means of one LVDT. This measurement is used to compute the radial strain ε_r, see Appendix 1. Moreover, the volumetric strain ε_{vol} is defined as

$$\varepsilon_{vol} = \varepsilon_a + 2\varepsilon_r$$

The stresses and the strains are defined as positive in compressive loading and deformation. The elasticity parameters are defined by the tangent Young's modulus E and tangent Poisson ratio ν as

$$E = \frac{\sigma_a(0.60\sigma_c) - \sigma_a(0.40\sigma_c)}{\varepsilon_a(0.60\sigma_c) - \varepsilon_a(0.40\sigma_c)}$$

$$\nu = -\frac{\varepsilon_r(0.60\sigma_c) - \varepsilon_r(0.40\sigma_c)}{\varepsilon_a(0.60\sigma_c) - \varepsilon_a(0.40\sigma_c)}$$

The tangents were evaluated with values corresponding to an axial load between 40 % and 60 % of the axial peak stress σ_c.

Two important observations can be made from the results:

(i) The results based on the total axial deformation measurement (S2) display a lower axial stiffness, i.e. a lower value on Young's modulus, than in the case when the results are based on the local axial deformation measurement (S1). This is due to the additional deformations from the contact interface between the rock specimen and the steel loading platens and also due to the deformation of the loading platens themselves.

(ii) It can be seen that the response differs qualitatively between the results obtained with the local axial deformation measurement system (S1) and the system that measures total axial deformation (S2). In some cases the post-peak response obtained with the local deformation measurement system seems not to be physically correct. This can be due to a number of reasons, e.g. that a crack caused a localized deformation, see Figure 5-1. Another explanation could be that the rings attached to the specimens have slightly slipped or moved, for example if a crack was formed nearby one of the attachment points.

It is reasonable to assume that results based on the local axial deformation measurement (S1) are fairly accurate up to the formation of the first macro-cracks or up to the peak load, but not thereafter. However, the results obtained with the total axial deformation measurement (S2) seem to be qualitatively correct after failure. We will therefore report the results based on the total axial deformation measurement, but carry out a correction of those results as described below in order to obtain overall good results.

The total axial deformation δ_{total} measured by (S2) is a summation of several deformations

$$\delta_{\text{total}} = \delta_{\text{rock}} + \delta_{\text{system}} \tag{5-1}$$

where

$$\delta_{\text{system}} = \delta_{\text{interface}} + \delta_{\text{loading platens}}$$

and δ_{rock} is the axial deformation of the whole rock specimen. Assume that the system deformation is proportional to the applied axial force F in the loading chain, i.e.

$$\delta_{\text{system}} = F/K_{\text{system}} \tag{5-2}$$

where K_{system} is the axial stiffness in the system (containing the interface between the rock and loading platens and the deformation of the loading platens). Combining (Equation 5-1) and (Equation 5-2) leads to

$$\delta_{\text{rock}} = \delta_{\text{total}} - F/K_{\text{system}} \tag{5-3}$$

where an expression of the axial deformation in the whole specimen is obtained. This can be viewed as a correction of the measurements made by system (S2). By using δ_{rock} to represent the axial deformation of the specimen that is based on a correction of the results of the total axial deformation will yield good results both in the loading range up to failure and at loading after failure. However, it is noticed that K_{system} is not known and has to be determined.

It was previously suggested that the local axial deformation measurement (S1) represents the real rock deformation well up to the load where the macro-cracks form. Further, it is fair to assume that the axial deformation is homogenous at this part of the loading. Hence, we get

$$\delta_{\text{rock}} = \delta_{\text{local}} \cdot L_{\text{total}}/L_{\text{local}} \tag{5-4}$$

This yields representative values of the total rock deformation for the first part of the loading up to the point where macro-cracking is taking place. It is now possible to determine δ_{system} up to the threshold of macro-cracking by combining (Equation 5-1) and (Equation 5-4) which yields

$$\delta_{\text{system}} = \delta_{\text{total}} - \delta_{\text{local}} \cdot L_{\text{total}}/L_{\text{local}} \tag{5-5}$$

Finally, we need to compute K_{system}. By rewriting (Equation 5-2) we get

$$K_{\text{system}} = \frac{F}{\delta_{\text{system}}}$$

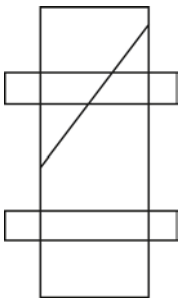

Figure 5-1. *Example of cracking that may cause results that are difficult to interpret with a local deformation measurement.*

We will compute the system stiffness based on the results between 40 % and 60 % of the axial peak stress σ_c. This means that the Young's modulus and the Poisson ratio will take the same values both when the data from the local axial deformation measurement (S1) and when the data from corrected total axial deformation are used. Thus, we have

$$K_{\text{system}} = \frac{F(0.60\sigma_c) - F(0.40\sigma_c)}{\delta_{\text{system}}(0.60\sigma_c) - \delta_{\text{system}}(0.40\sigma_c)} \tag{5-6}$$

The results based on the correction according to (Equation 5-3) and (Equation 5-6) are presented in Section 6.4, whereas the original measured unprocessed data are reported in Appendix 2.

A closure of present micro-cracks will take place initially during axial loading. Development of new micro-cracks will start when the load is further increased and axial stress reaches the crack initiation stress σ_i. The crack growth at this stage is as stable as increased loading is required for further cracking. A transition from a development of micro-cracks to macro-cracks will occur when the axial load is further increased. At a certain stress level the crack growth becomes unstable. The stress level when this happens is denoted the crack damage stress σ_d, cf. Martin and Chandler (1994). In order to determine the stress levels, we look at the volumetric strain.

By subtracting the elastic volumetric strain ε^{e}_{vol} from the total volumetric strain, a volumetric strain corresponding to the crack volume ε^{cr}_{vol} is obtained. This has been denoted calculated crack volumetric strain in the literature, cf. Martin and Chandler (1994) and Eberhardt et al. (1998). We thus have

$$\varepsilon^{\text{cr}}_{\text{vol}} = \varepsilon_{\text{vol}} - \varepsilon^{\text{e}}_{\text{vol}}$$

Assuming linear elasticity leads to

$$\varepsilon^{\text{cr}}_{\text{vol}} = \varepsilon_{\text{vol}} - \frac{1-2\upsilon}{E}\sigma_a$$

where $\sigma_r = 0$ was used. Experimental investigations have shown that the crack initiation stress σ_i coincides with the onset of increase of the calculated crack volume, cf. Martin and Chandler (1994) and Eberhardt et al. (1998). The same investigations also indicate that the crack damage stress σ_d can be defined as the axial stress at which the total volume starts to increase, i.e. when a dilatant behaviour is observed.

Another method to assess the crack initiation stress based on strain measurements is to use the Inverse Tangent Lateral Stiffness, cf. Ghazvinian et al. (2012), which was used in e.g. Jacobsson et al. (2016).

5.6 Data handling

The test results were transferred to and stored in a file server on the RISE computer network after completed tests. The main data processing, in which the elastic moduli were computed and the peak stress was determined, has been carried out using the program MATLAB, MathWorks (2014). Moreover, MATLAB was used to produce the diagrams shown in Section 6.4 and in Appendix 2. MS Excel was used to produce the other diagrams and for reporting data to the SICADA database.

5.7 Nonconformities

The testing was conducted according to the method description with some deviations. The circumferential strains have been determined within a relative error of 1.5 %, which is larger than what is specified in the ISRM-standard (ISRM 1999). Further, double systems for measuring the axial deformation have been used, which is beyond the specifications in the method description. This was conducted as development of the test method specially aimed for high-strength brittle rock.

The activity plan was followed with no departures.

6 Results

The reported parameters are based both on unprocessed raw data obtained from the testing and processed data and were reported to the Sicada database, where they are traceable by the activity plan number. These data together with the digital photographs of the individual specimens were handed over to SKB. The handling of the results follows SDP-508 (SKB internal controlling document) in general.

6.1 Density

The density of the specimens at a water saturated condition is shown in the results tables for the mechanical tests in Sections 6.3 and 6.4. An overview of the results for all specimens is shown in Figure 6-1.

6.2 Transient plane source

6.2.1 Results for each individual specimen

The average results of at least 6 individual measurements for each interface measured are presented in Table 6-1along with the standard deviations between individual measurements in Table 6-2. Standard deviation of measured values at 22 °C.Table 6-2. The standard deviations are less than 1.4 % for conductivity (median 0.4 %), 1.5 % for diffusivity (median 0.8 %) and 4.1 % for volumetric specific heat (median 1.3 %).

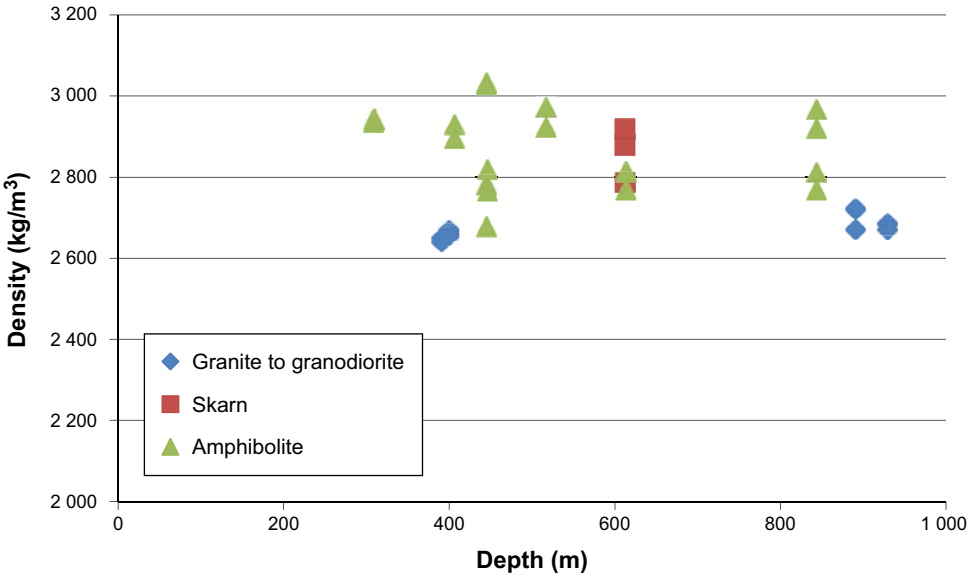

Figure 6-1. *Density as a function of depth for the three rock types in the study.*

Table 6-1. Mean value of thermal properties of samples at 22 °C. All measurements were 40 s long.

Identification	Heating power [mW]	Points analyzed	Conductivity [W/(m, K)]	Diffusivity [mm²/s]	Heat capacity [MJ/(m³, K)]	No. of measurements
KFM01A 90V 01	700	50–120	3.384	1.649	2.052	10
KFM01A 90V 02	700	50–110	3.391	1.755	1.933	10
KFM01A 90V 03	350	90–180	1.570	0.902	1.740	10
KFM01A 90V 04	350	80–160	1.813	1.091	1.661	10
KFM01A 90V 05	350	80–160	2.187	1.064	2.056	10
KFM01A 90V 06	500	80–160	2.597	1.014	2.623	10
KFM01A 90V 07	500	50–100	3.379	1.910	1.772	7
KFM01A 90V 08	500	40–110	3.416	1.712	1.995	10
KFM04A 90V 09	500	40–160	3.453	1.425	2.424	12
KFM04A 90V 10	500	50–130	3.477	1.497	2.323	12
KFM04A 90V 11	500	50–130	2.395	1.170	2.048	12
KFM04A 90V 12	500	50–100	3.254	1.822	1.787	6
KFM04A 90V 13	500	40–110	2.646	1.256	2.107	6
KFM04A 90V 14	500	60–140	2.826	1.299	2.175	12
KFM05A 90V 15	500	60–190	2.205	0.879	2.510	7
KFM05A 90V 16	500	50–100	3.298	1.828	1.810	12
KFM05A 90V 17	500	50–100	3.380	1.686	2.005	12
KFM24 90V 18	500	50–100	3.622	1.860	1.948	12
KFM24 90V 19	500	60–100	2.699	1.699	1.589	12
KFM24 90V 20	500	40–180	2.197	1.000	2.198	11

Table 6-2. Standard deviation of measured values at 22 °C.

Identification	Conductivity [W/(m, K)]	Diffusivity [mm²/s]	Heat capacity [MJ/(m³, K)]
KFM01A 90V 01	0.0242	0.0257	0.0379
KFM01A 90V 02	0.0219	0.0293	0.0387
KFM01A 90V 03	0.0116	0.0090	0.0173
KFM01A 90V 04	0.0027	0.0077	0.0104
KFM01A 90V 05	0.0016	0.0054	0.0115
KFM01A 90V 06	0.0024	0.0060	0.0172
KFM01A 90V 07	0.0483	0.0574	0.0732
KFM01A 90V 08	0.0135	0.0171	0.0282
KFM04A 90V 09	0.0254	0.0231	0.0583
KFM04A 90V 10	0.0126	0.0113	0.0256
KFM04A 90V 11	0.0013	0.0013	0.0070
KFM04A 90V 12	0.0110	0.0253	0.0303
KFM04A 90V 13	0.0092	0.0084	0.0168
KFM04A 90V 14	0.0057	0.0080	0.0170
KFM05A 90V 15	0.0110	0.0105	0.0420
KFM05A 90V 16	0.0173	0.0223	0.0320
KFM05A 90V 17	0.0112	0.0122	0.0213
KFM24 90V 18	0.0178	0.0270	0.0378
KFM24 90V 19	0.0119	0.0214	0.0261
KFM24 90V 20	0.0080	0.0075	0.0244

6.2.2 Results for the entire test series

The thermal conductivity and thermal diffusivity of specimens representing different depths at 22 °C were in the range 1.6–3.6 W/(m, K) and 0.9–1.9 mm^2/s. From these results the volumetric heat capacity was calculated to range between 1.6 and 2.6 $MJ/(m^3, K)$. Graphical representation of the thermal conductivity and heat capacity versus borehole depth are given in Figures 6-2 and 6-3, respectively. There is a minimum in the thermal conductivity at about 600 of *k = 1.5–2* W/(m, K) and the influence from the rock types is probably large.

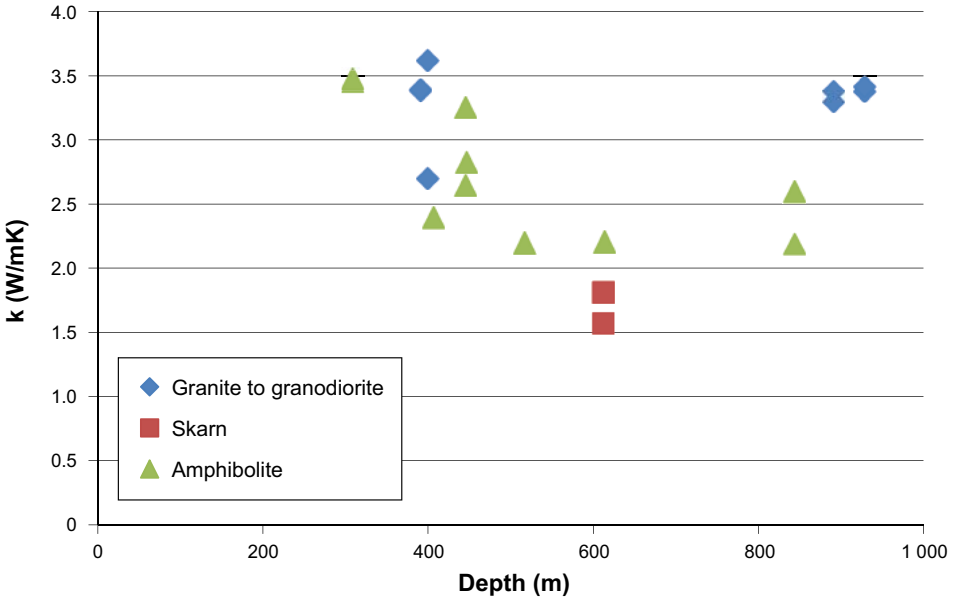

Figure 6-2. *Thermal conductivity as a function of depth for the three different rock types.*

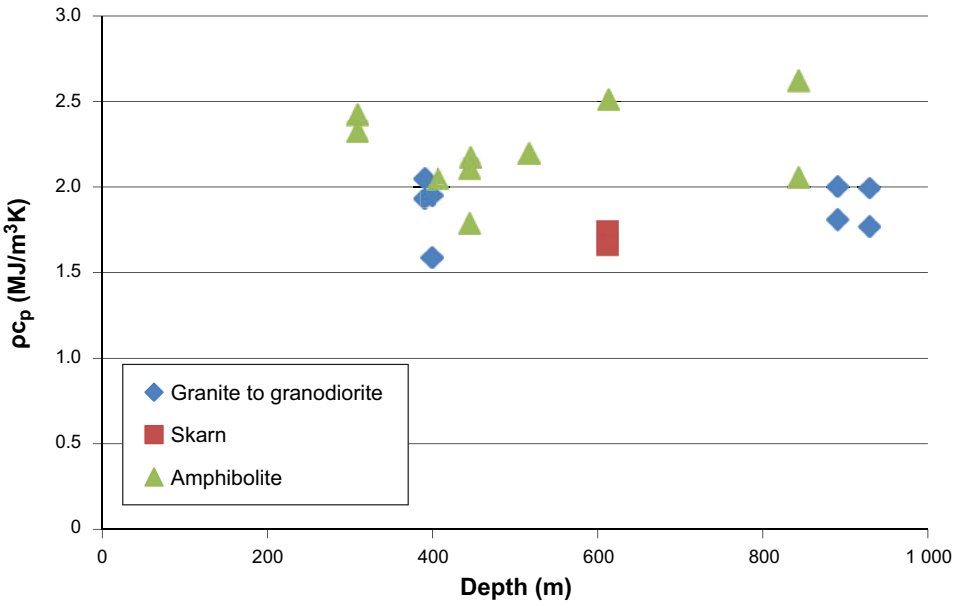

Figure 6-3. *Volumetric heat capacity as a function of depth for the three different rock types.*

6.3 Indirect tensile strength test

6.3.1 Results for each individual specimen

The results and photographs for the individual specimen are presented below.

Specimen ID: KFM01A-110-01

Before mechanical test

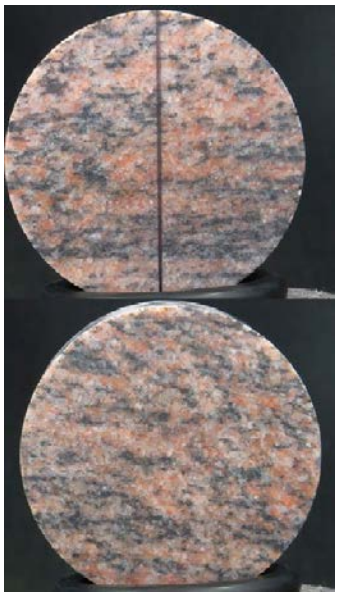

After mechanical test

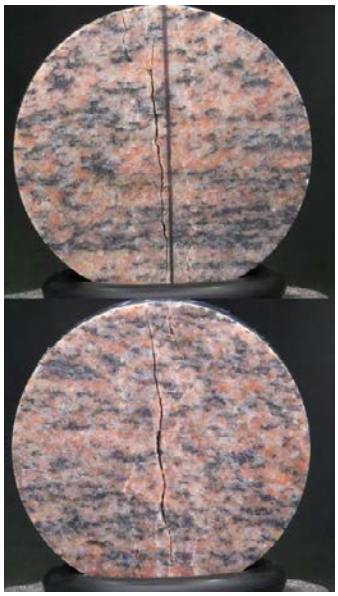

Diameter (mm)	Height (mm)	Density (kg/m^3)	Tensile strength (MPa)
50.9	25.7	2648	14.5

Comments: None

Specimen ID: KFM01A-110-02

Before mechanical test

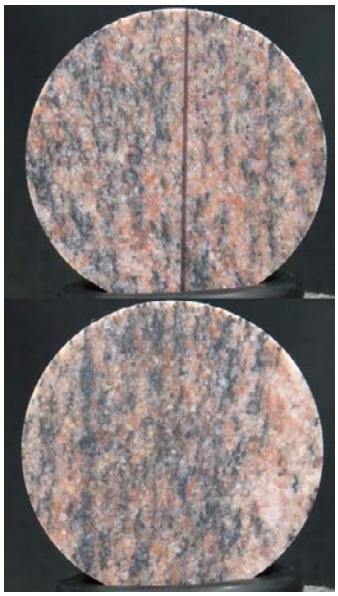

After mechanical test

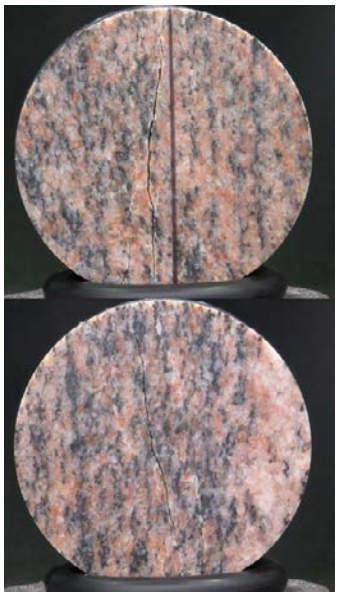

Diameter (mm)	Height (mm)	Density (kg/m^3)	Tensile strength (MPa)
50.9	25.7	2649	11.9

Comments: None

Specimen ID: KFM01A-110-03

Before mechanical test

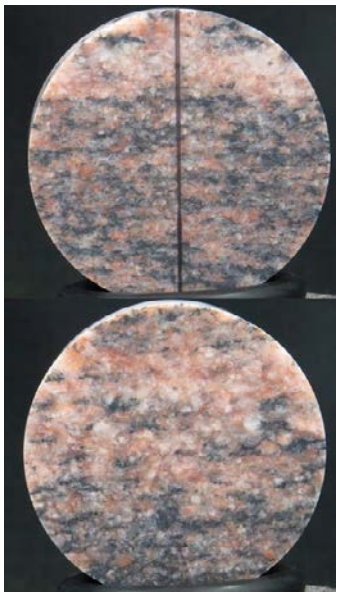

After mechanical test

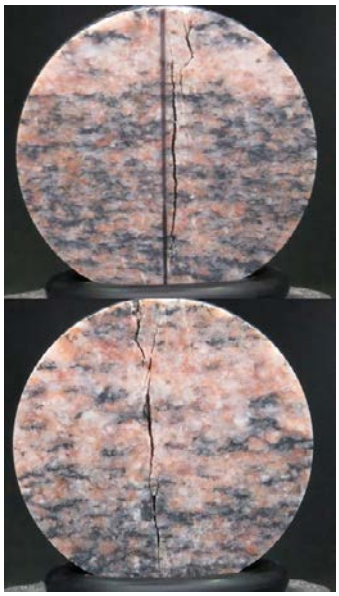

Diameter (mm)	Height (mm)	Density (kg/m^3)	Tensile strength (MPa)
50.9	26.6	2640	13.7

Comments: None

Specimen ID: KFM01A-110-04

Before mechanical test

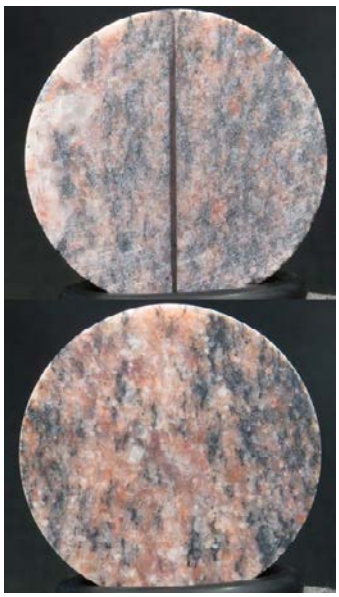

After mechanical test

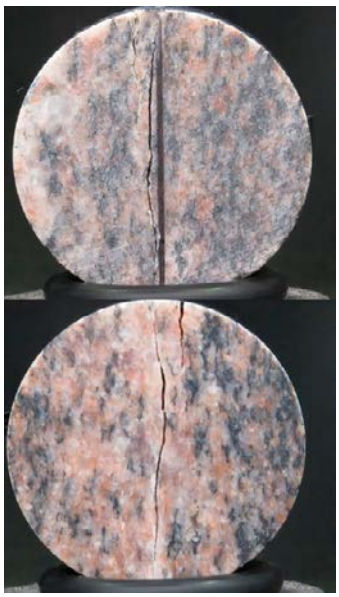

Diameter (mm)	Height (mm)	Density (kg/m^3)	Tensile strength (MPa)
50.9	25.4	2640	12.0

Comments: None

Specimen ID: KFM01A-110-05

Before mechanical test

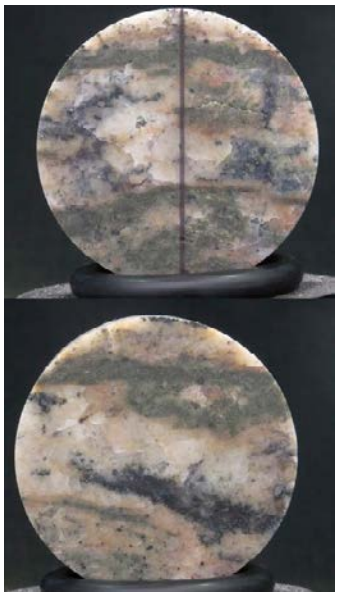

After mechanical test

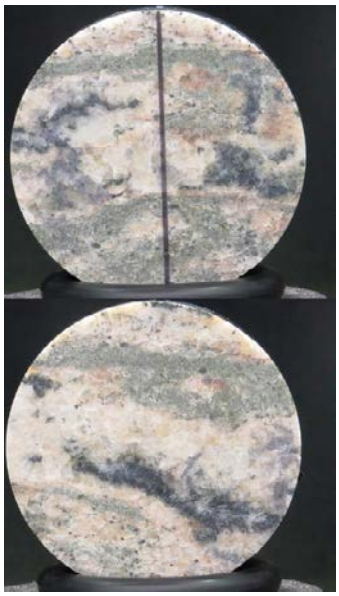

Diameter (mm)	Height (mm)	Density (kg/m^3)	Tensile strength (MPa)
50.7	25.6	2787	4.49

Comments: None

Specimen ID: KFM01A-110-06

Before mechanical test

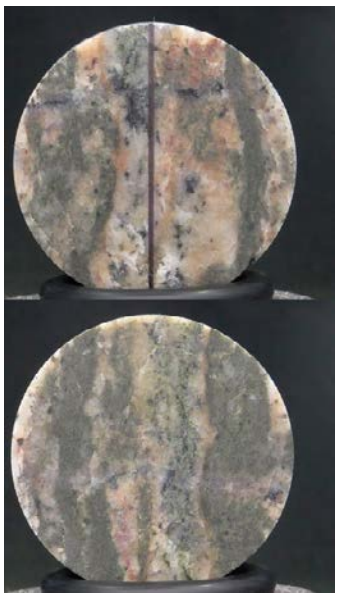

After mechanical test

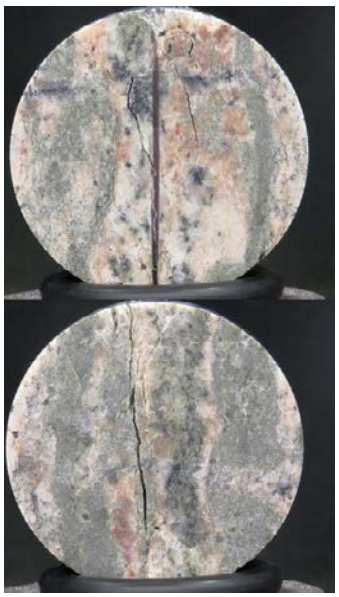

Diameter (mm)	Height (mm)	Density (kg/m^3)	Tensile strength (MPa)
50.7	25.7	2878	6.45

Comments: None

Specimen ID: KFM01A-110-07

Before mechanical test

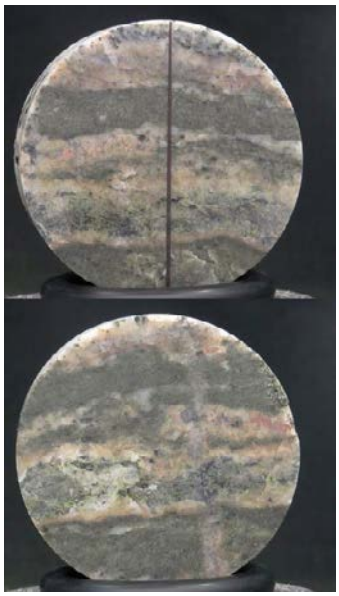

After mechanical test

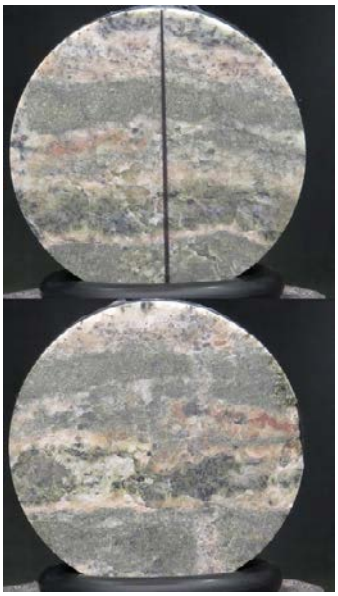

Diameter (mm)	Height (mm)	Density (kg/m^3)	Tensile strength (MPa)
50.7	26.4	2915	5.62

Comments: None

Specimen ID: KFM01A-110-08

Before mechanical test

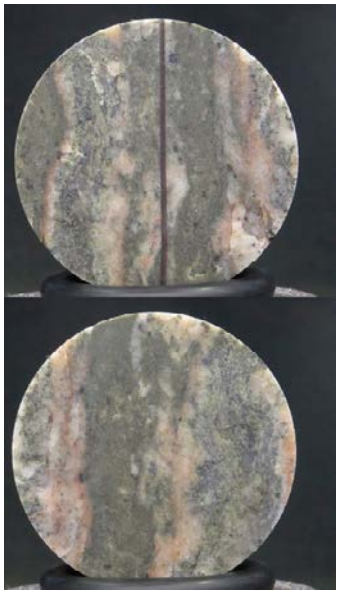

After mechanical test

Diameter (mm)	Height (mm)	Density (kg/m^3)	Tensile strength (MPa)
50.7	26.2	2920	8.51

Comments: None

Specimen ID: KFM01A-110-09

Before mechanical test

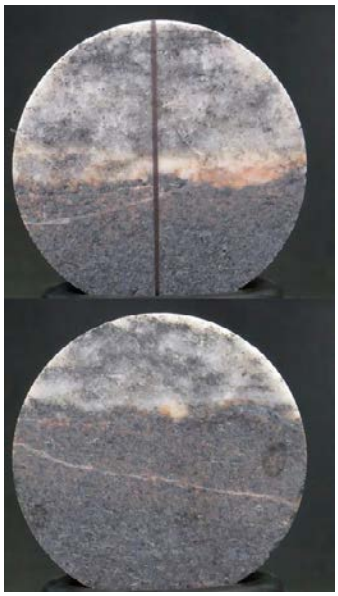

After mechanical test

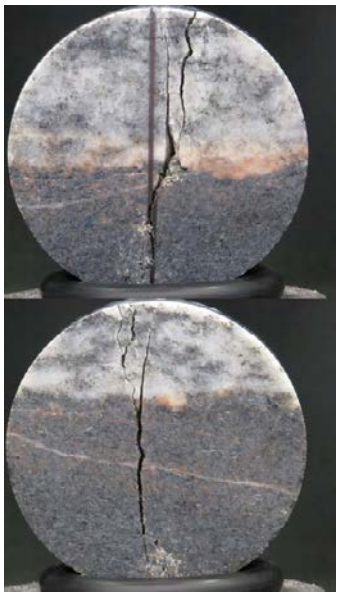

Diameter (mm)	Height (mm)	Density (kg/m^3)	Tensile strength (MPa)
50.7	25.8	2768	14.0

Comments: None

Specimen ID: KFM01A-110-10

Before mechanical test

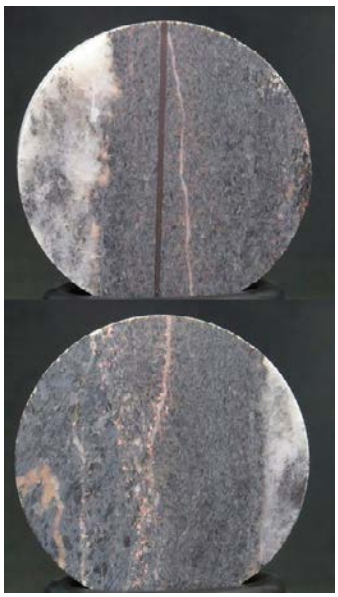

After mechanical test

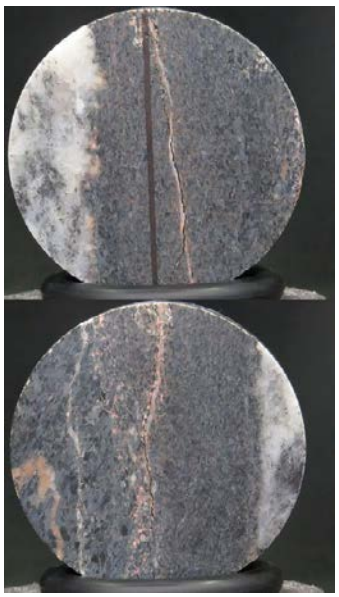

Diameter (mm)	Height (mm)	Density (kg/m^3)	Tensile strength (MPa)
50.7	25.3	2812	8.39

Comments: None

Specimen ID: KFM01A-110-11

Before mechanical test

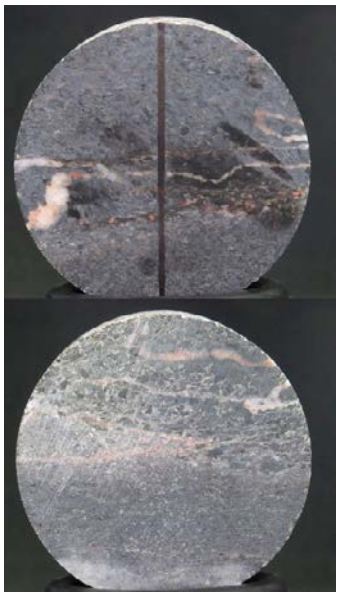

After mechanical test

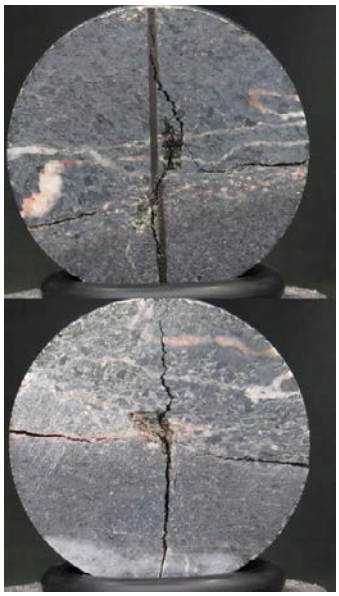

Diameter (mm)	Height (mm)	Density (kg/m^3)	Tensile strength (MPa)
50.8	26.4	2920	11.6

Comments: None

Specimen ID: KFM01A-110-12

Before mechanical test

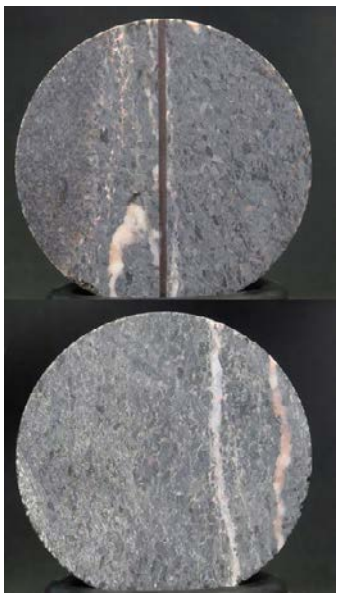

After mechanical test

Diameter (mm)	Height (mm)	Density (kg/m^3)	Tensile strength (MPa)
50.9	26.3	2967	7.13

Comments: Cracking at loading surface at 5.4 MPa

Specimen ID: KFM01A-110-13

Before mechanical test

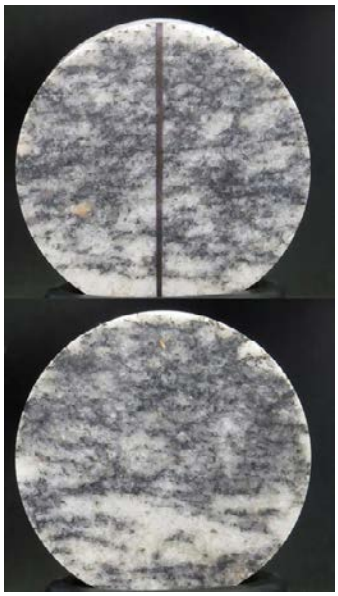

After mechanical test

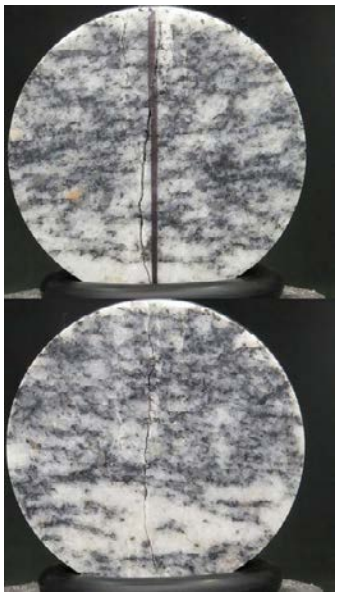

Diameter (mm)	Height (mm)	Density (kg/m^3)	Tensile strength (MPa)
50.9	25.4	2685	11.8

Comments: None

Specimen ID: KFM01A-110-14

Before mechanical test

After mechanical test

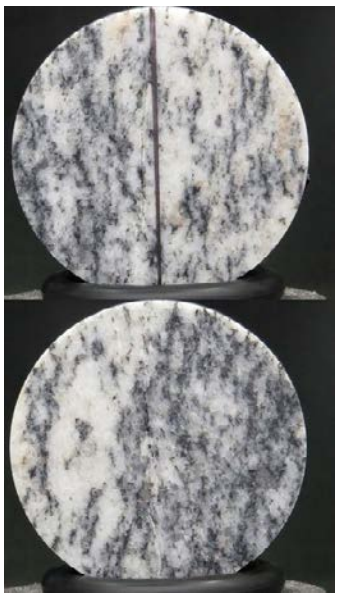

Diameter (mm)	Height (mm)	Density (kg/m^3)	Tensile strength (MPa)
50.9	25.4	2682	8.48

Comments: None

Specimen ID: KFM01A-110-15

Before mechanical test

After mechanical test

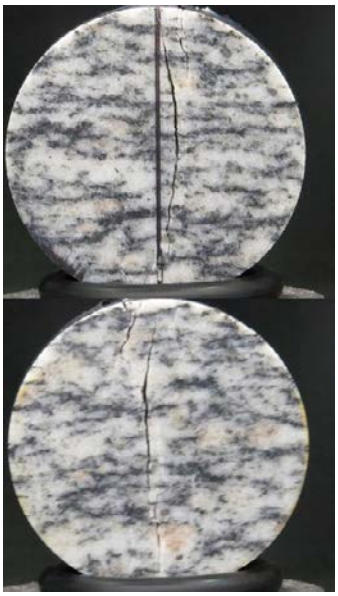

Diameter (mm)	Height (mm)	Density (kg/m^3)	Tensile strength (MPa)
50.9	26.0	2671	12.8

Comments: None

Specimen ID: KFM01A-110-16

Before mechanical test

After mechanical test

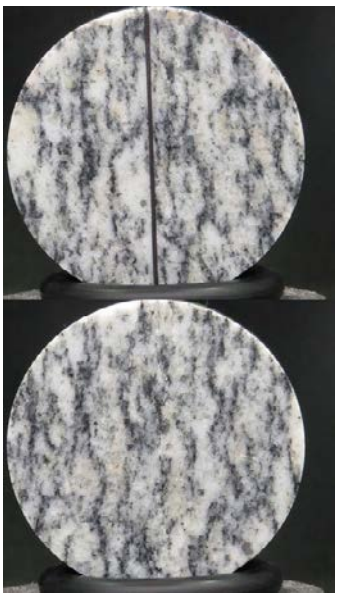

Diameter (mm)	Height (mm)	Density (kg/m^3)	Tensile strength (MPa)
50.9	26.0	2670	8.07

Comments: None

Specimen ID: KFM04A-110-17

Before mechanical test

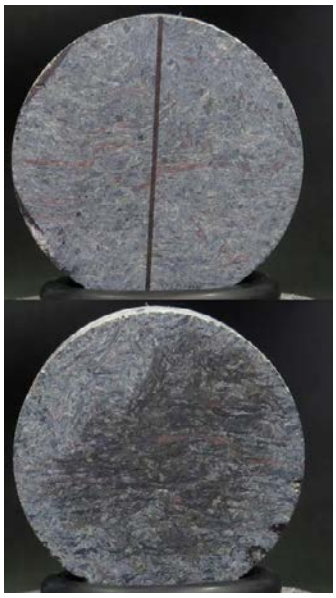

After mechanical test

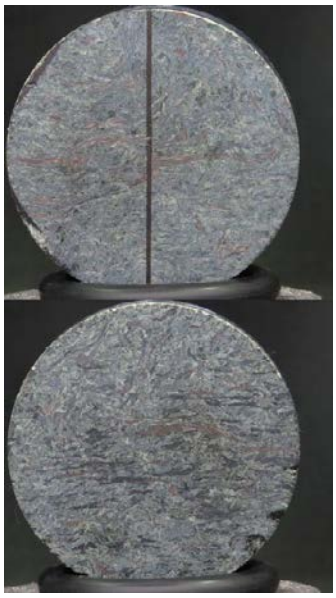

Diameter (mm)	Height (mm)	Density (kg/m^3)	Tensile strength (MPa)
50.8	26.1	2935	1.74

Comments: Crack curves out to the horizontal foliation direction

Specimen ID: KFM04A-110-18

Before mechanical test

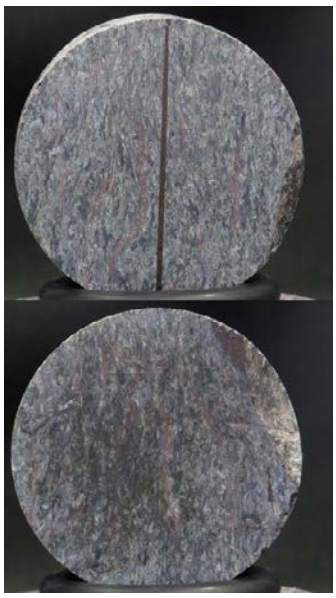

After mechanical test

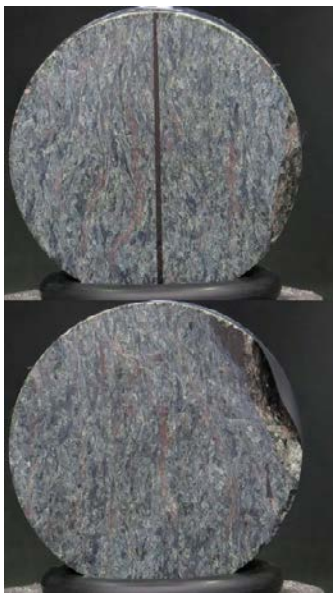

Diameter (mm)	Height (mm)	Density (kg/m^3)	Tensile strength (MPa)
50.8	26.0	2941	2.11

Comments: None

Specimen ID: KFM04A-110-19

Before mechanical test

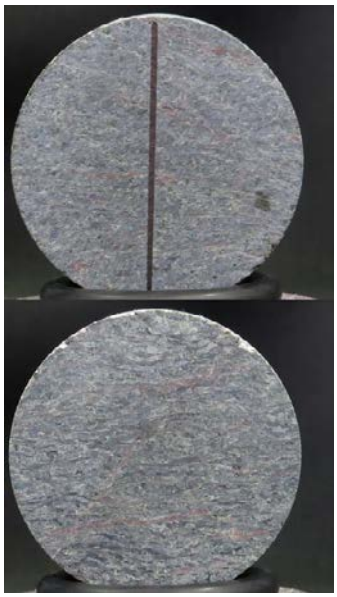

After mechanical test

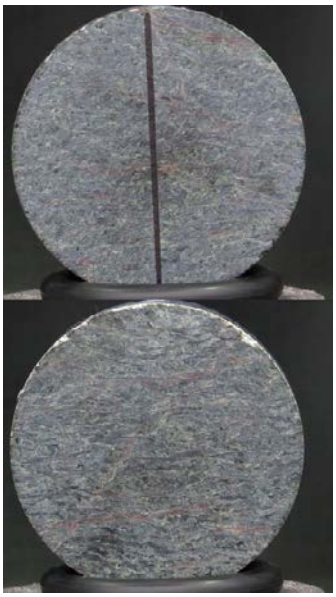

Diameter (mm)	Height (mm)	Density (kg/m^3)	Tensile strength (MPa)
50.8	25.8	2941	2.16

Comments: Approximately horizontal crack along foliation

Specimen ID: KFM04A-110-20

Before mechanical test

After mechanical test

Diameter (mm)	Height (mm)	Density (kg/m^3)	Tensile strength (MPa)
50.8	25.9	2944	1.18

Comments: None

Specimen ID: KFM04A-110-1b

Before mechanical test

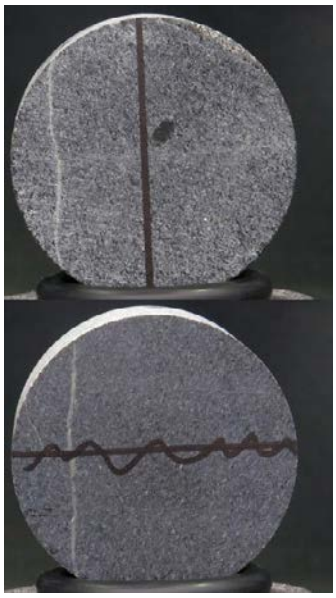

After mechanical test

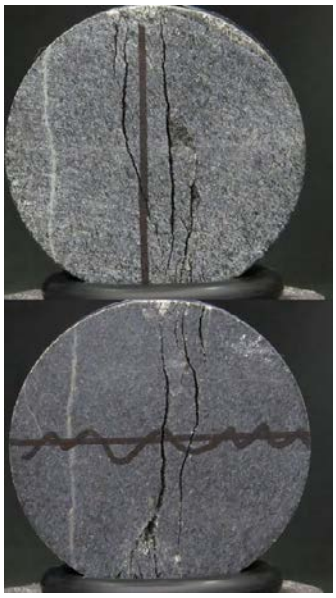

Diameter (mm)	Height (mm)	Density (kg/m^3)	Tensile strength (MPa)
50.9	26.1	2929	16.2

Comments: None

Specimen ID: KFM04A-110-21

Before mechanical test

After mechanical test

Diameter (mm)	Height (mm)	Density (kg/m^3)	Tensile strength (MPa)
50.8	25.5	2678	5.10

Comments: Failure in sealed joint

Specimen ID: KFM04A-110-22

Before mechanical test

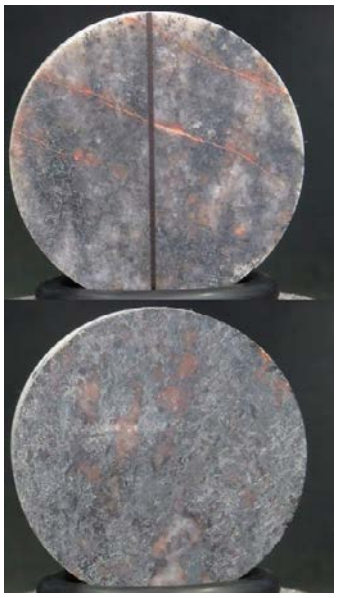

After mechanical test

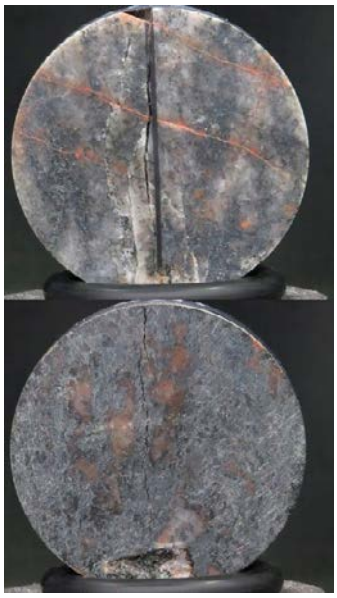

Diameter (mm)	Height (mm)	Density (kg/m^3)	Tensile strength (MPa)
50.8	25.3	2781	14.7

Comments: None

Specimen ID: KFM04A-110-23

Before mechanical test

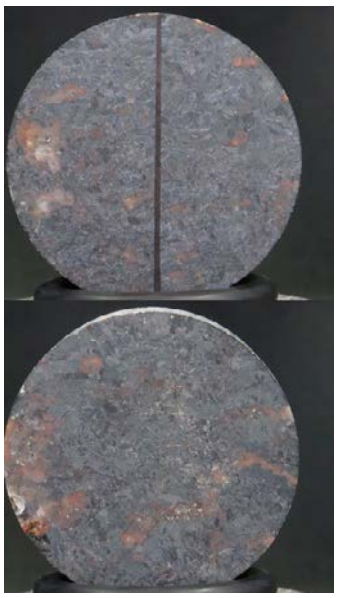

After mechanical test

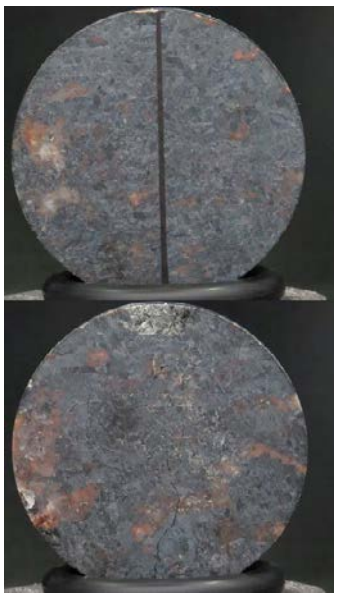

Diameter (mm)	Height (mm)	Density (kg/m^3)	Tensile strength (MPa)
50.8	25.4	3033	9.36

Comments: None

Specimen ID: KFM04A-110-24

Before mechanical test

After mechanical test

Diameter (mm)	Height (mm)	Density (kg/m^3)	Tensile strength (MPa)
50.8	25.5	3028	10.5

Comments: None

Specimen ID: KFM04A-110-2b

Before mechanical test

After mechanical test

Diameter (mm)	Height (mm)	Density (kg/m^3)	Tensile strength (MPa)
50.8	26.5	2819	11.1

Comments: None

Specimen ID: KFM05A-110-28

Before mechanical test

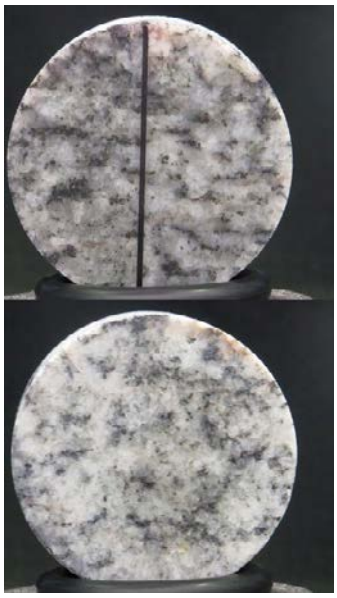

After mechanical test

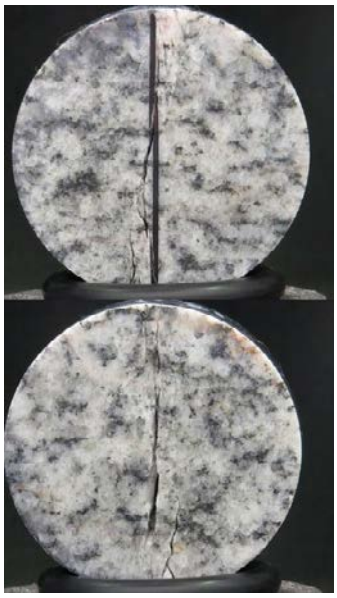

Diameter (mm)	Height (mm)	Density (kg/m^3)	Tensile strength (MPa)
50.6	26.0	2719	10.9

Comments: None

Specimen ID: KFM05A-110-29

Before mechanical test

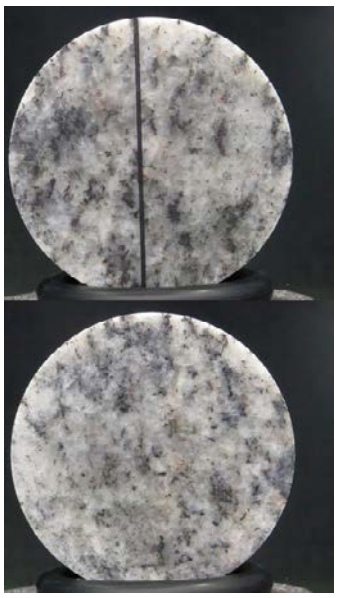

After mechanical test

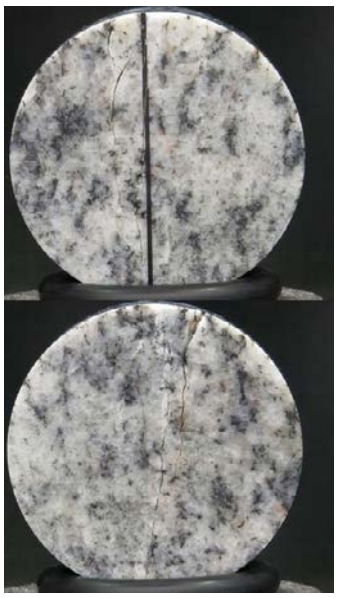

Diameter (mm)	Height (mm)	Density (kg/m^3)	Tensile strength (MPa)
50.3	26.1	2722	10.0

Comments: Small load drop at 6.24 MPa

Specimen ID: KFM05A-110-30

Before mechanical test

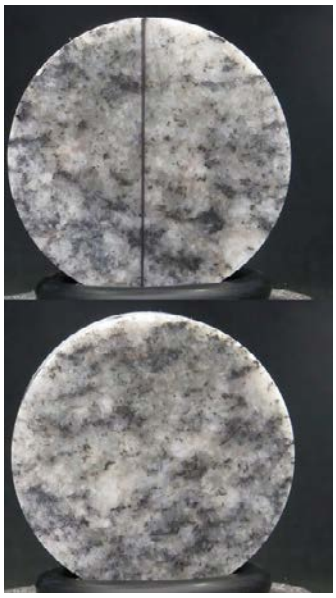

After mechanical test

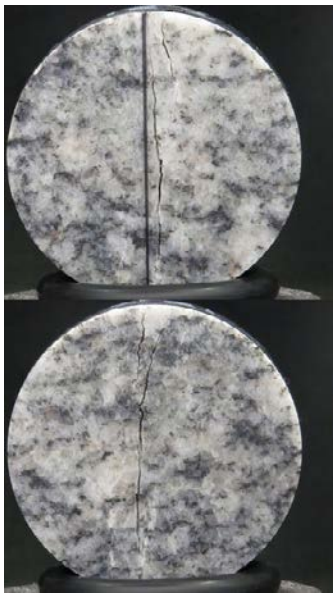

Diameter (mm)	Height (mm)	Density (kg/m^3)	Tensile strength (MPa)
50.3	26.1	2671	11.6

Comments: None

Specimen ID: KFM05A-110-31

Before mechanical test

After mechanical test

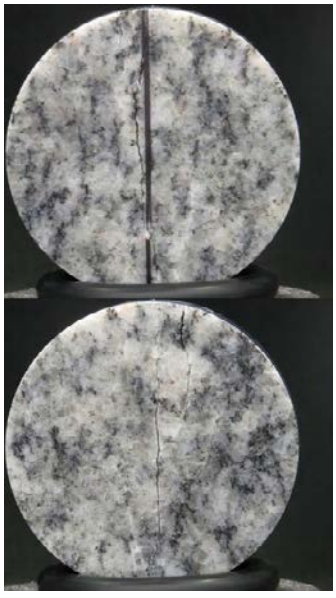

Diameter (mm)	Height (mm)	Density (kg/m^3)	Tensile strength (MPa)
50.3	26.2	2672	10.1

Comments: None

Specimen ID: KFM24-110-32

Before mechanical test

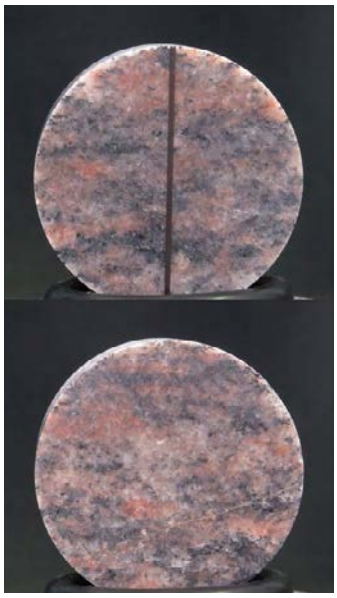

After mechanical test

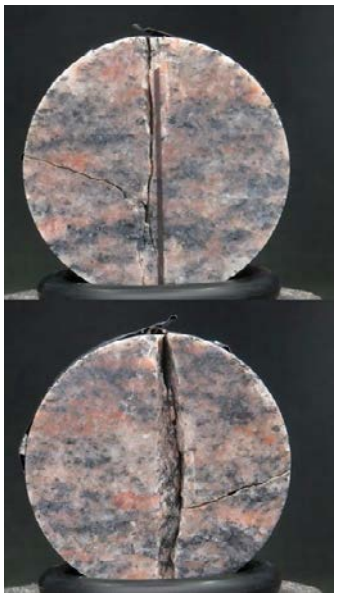

Diameter (mm)	Height (mm)	Density (kg/m^3)	Tensile strength (MPa)
45.3	25.8	2668	13.1

Comments: None

Specimen ID: KFM24-110-33

Before mechanical test

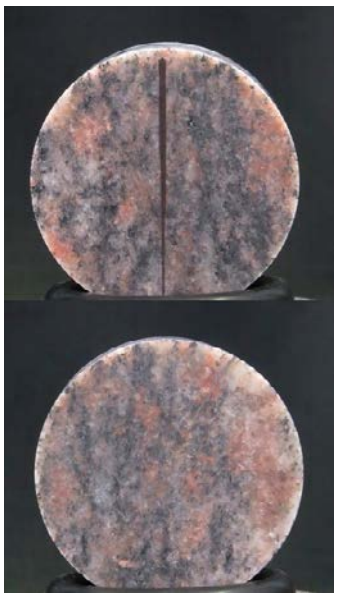

After mechanical test

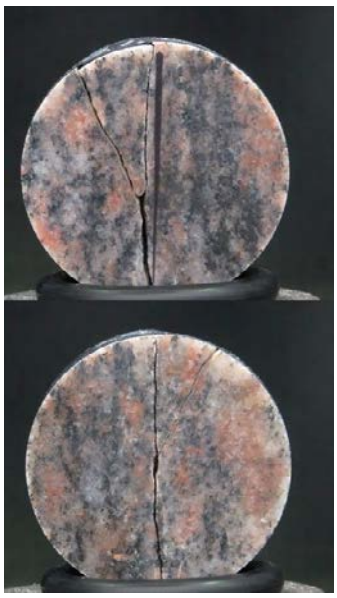

Diameter (mm)	Height (mm)	Density (kg/m^3)	Tensile strength (MPa)
45.2	25.8	2669	11.5

Comments: None

Specimen ID: KFM24-110-34

Before mechanical test

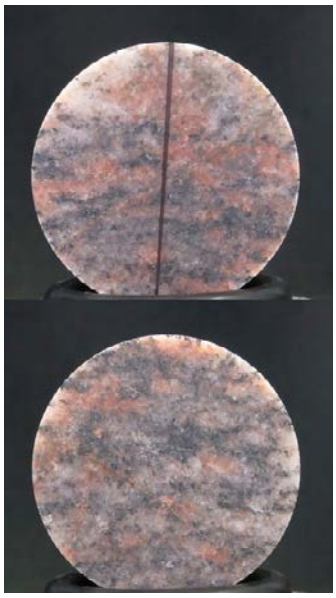

After mechanical test

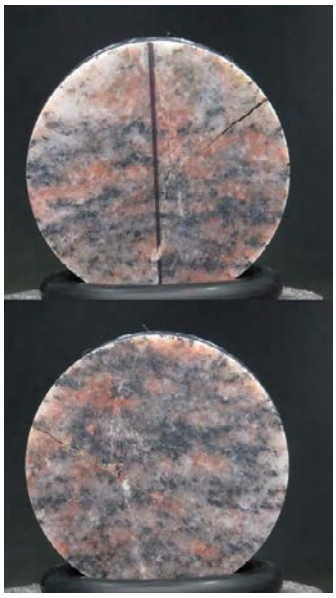

Diameter (mm)	Height (mm)	Density (kg/m^3)	Tensile strength (MPa)
45.2	26.0	2660	11.6

Comments: None

Specimen ID: KFM24-110-35

Before mechanical test

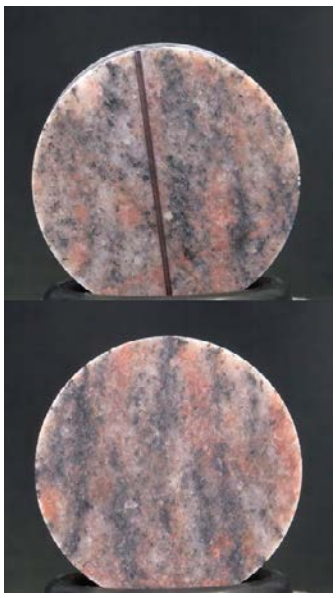

After mechanical test

Diameter (mm)	Height (mm)	Density (kg/m^3)	Tensile strength (MPa)
45.2	26.1	2655	10.9

Comments: Specimen fractured at c 30 deg inclination to the load line

Specimen ID: KFM24-110-3b

Before mechanical test

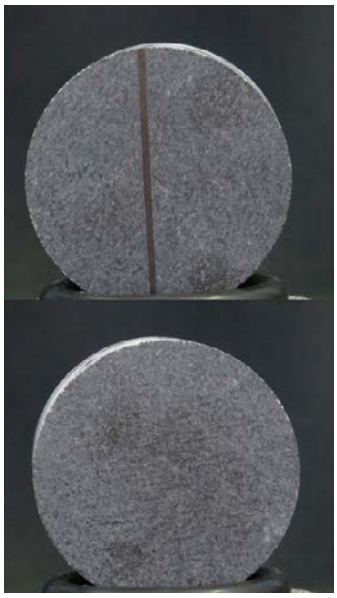

After mechanical test

Diameter (mm)	Height (mm)	Density (kg/m^3)	Tensile strength (MPa)
44.9	26.4	2973	16.0

Comments: None

6.3.2 Results for the entire test series

The test results are shown in Tables 6-3.

The amphibolite specimens KFM04A-110-17 to KFM04A-110-20, core number 7 (Figure 3-2) display a low indirect tensile strength (1.18–2.16 MPa) in both loading along and perpendicular to the foliation. The geologist in Forsmark made the following note when the cores were collected for the core boxes: amphibolite, green foliated, chlorite altered with some slim healed oxidised cracks. From the photos of the individual specimens in Section 6.3.1 it can be observed that the grains are much elongated in the foliation direction. Furthermore is seems that the rock is in the direction towards monzodiorite, whereby it is likely to contain biotite which lowers the strength. A detailed study of the actual rock specimens is needed to confirm the assumptions.

Table 6-3. Results from density measurements and direct tensile tests.

Identification	Density (kg/m^3)	Tensile strength (MPa)	Comments
KFM01A-110-01	2648	14.5	PF (PF = load line perpendicular to foliation)
KFM01A-110-02	2649	11.9	AF (AF = load line along foliation)
KFM01A-110-03	2640	13.7	PF
KFM01A-110-04	2640	12.0	AF
KFM01A-110-05	2787	4.49	PF
KFM01A-110-06	2878	6.45	AF
KFM01A-110-07	2915	5.62	PF
KFM01A-110-08	2920	8.51	AF
KFM01A-110-09	2768	14.0	PF
KFM01A-110-10	2812	8.39	AF
KFM01A-110-11	2920	11.6	PF
KFM01A-110-12	2967	7.13	AF, cracking at loading surface at 5.4 MPa
KFM01A-110-13	2685	11.8	PF
KFM01A-110-14	2682	8.48	AF
KFM01A-110-15	2671	12.8	PF
KFM01A-110-16	2670	8.07	AF
KFM04A-110-17	2935	1.74	PF, crack curves out to foliation direction
KFM04A-110-18	2941	2.11	AF
KFM04A-110-19	2941	2.16	PF, approx. horozontal crack along foliation
KFM04A-110-20	2944	1.18	AF
KFM04A-110-1b	2929	16.2	PF
KFM04A-110-21	2678	5.10	PF, failure in sealed joint
KFM04A-110-22	2781	14.7	AF
KFM04A-110-23	3033	9.36	PF
KFM04A-110-24	3028	10.5	AF
KFM04A-110-2b	2819	11.1	PF
KFM05A-110-25	2813	–	Defect specimen
KFM05A-110-26	2814	–	Defect specimen
KFM05A-110-27	2768	–	Defect specimen
KFM05A-110-28	2719	10.9	PF
KFM05A-110-29	2722	10.0	AF, small load drop at 6.24 MPa
KFM05A-110-30	2671	11.6	PF
KFM05A-110-31	2672	10.1	AF
KFM24-110-32	2668	13.1	PF
KFM24-110-33	2669	11.5	AF
KFM24-110-34	2660	11.6	PF
KFM24-110-35	2655	10.9	AF, fracture c 30 deg inclination to the load line
KFM24-110-3b	2973	16.0	PF

6.4 Uniaxial compression test

6.4.1 Results for each individual specimen

The cracking is shown in photos of the specimens, and comments on observations made during the testing are reported. The elasticity parameters have been evaluated by using the results from the local axial deformation measurements. The data from the adjusted total axial deformation measurements, cf. Section 5.5.2, are shown in this section.

Diagrams showing the data from both the local and the total axial deformation measurements, system (S1) and (S2) in Figure 4-5, and the computed individual values of K_{system} used at the data corrections are shown in Appendix 2. Diagrams displaying actual radial strain rates versus the test time are also presented in Appendix 2. The results for the individual specimens are as follows:

Specimen ID: KFM01A-113-1

Before mechanical test After mechanical test

Diameter (mm)	Height (mm)	Density (kg/m^3)
50.9	127.1	2895
Comments:	Steep diagonal failure.	

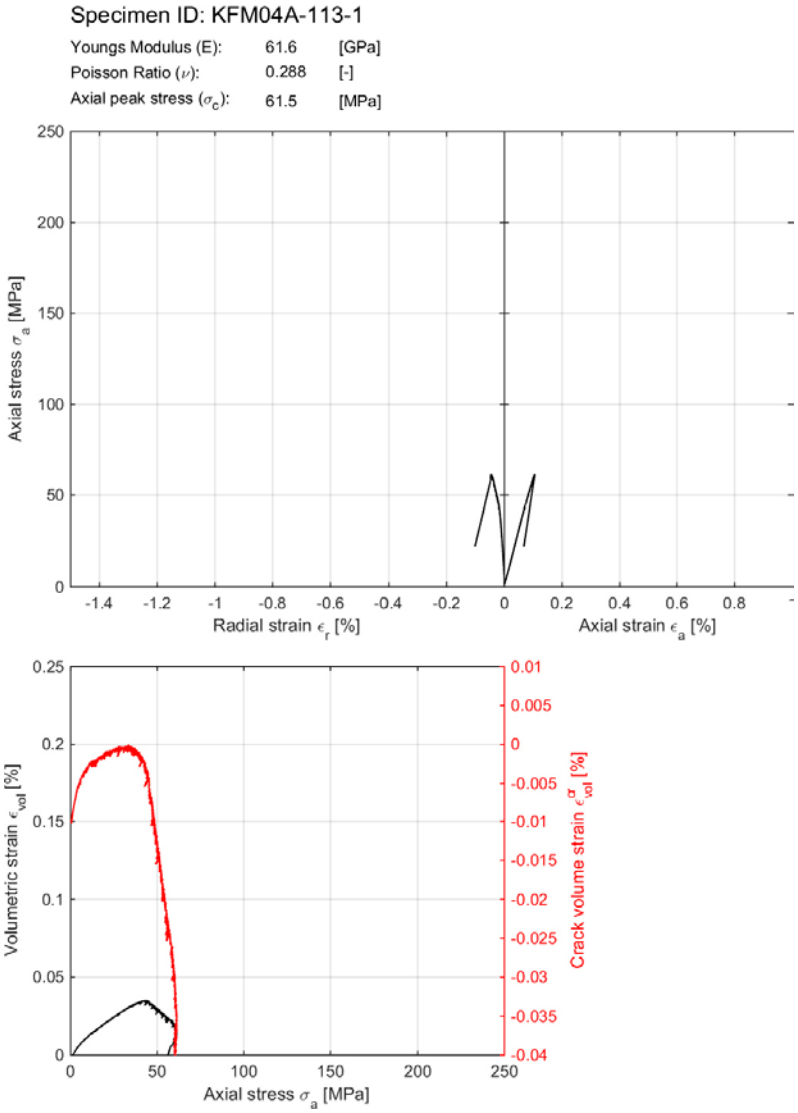

Specimen ID: KFM01A-113-2

Before mechanical test

After mechanical test

Diameter (mm)	Height (mm)	Density (kg/m^3)
50.8	127.0	2766
Comments:	Steep diagonal failure in an existing weakness plane or joint.	

Specimen ID: KFM04A-113-2

Youngs Modulus (E):	57.5	[GPa]
Poisson Ratio (ν):	0.407	[-]
Axial peak stress (σ_c):	68.5	[MPa]

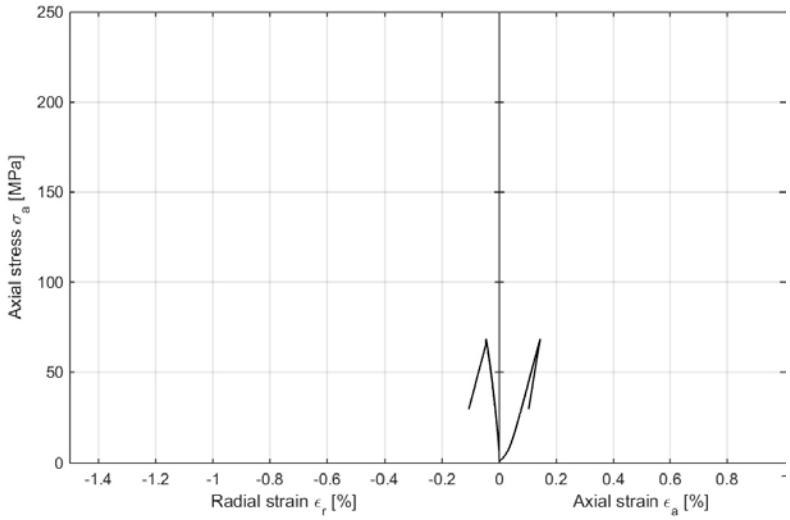

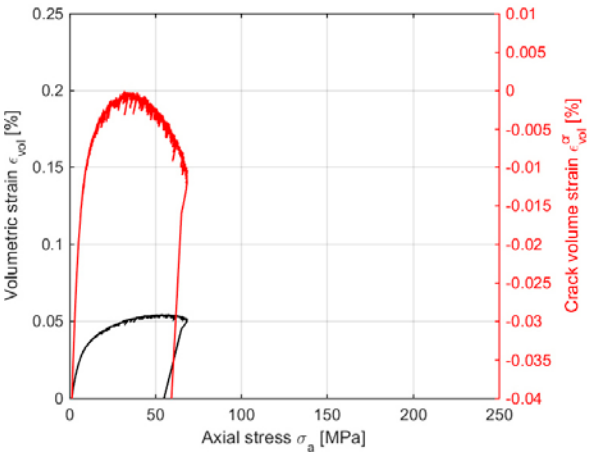

Specimen ID: KFM24-113-3

Before mechanical test

After mechanical test

Diameter (mm)	Height (mm)	Density (kg/m^3)
50.9	128.1	2923
Comments:	Spalling in the middle of one side of the specimen.	

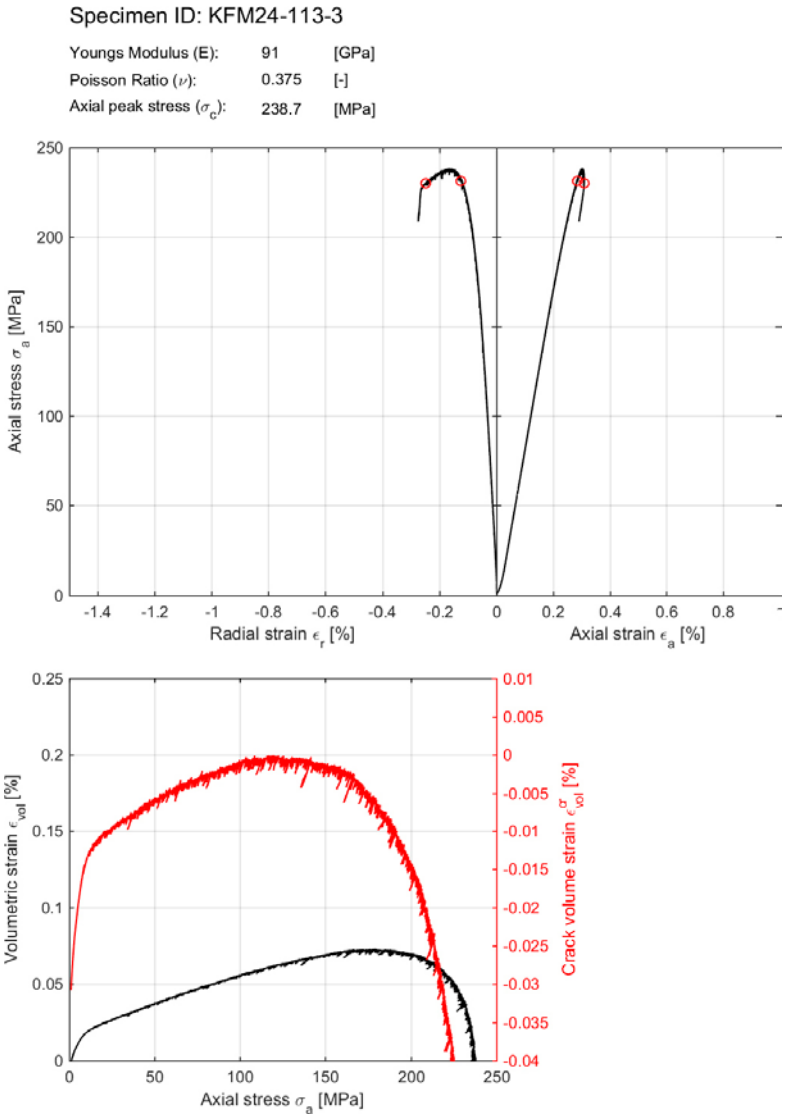

6.4.2 Results for the entire test series

A summary of the test results is shown in Table 6-4.

Table 6-4. Results from density measurements and uniaxial compression tests.

Identification	Density (kg/m^3)	Compressive strength (MPa)	Young's modulus (GPa)	Poisson ratio (–)
KFM01A-113-1	2895	61.5	61.6	0.288
KFM01A-113-2	2766	68.5	57.5	0.407
KFM24-113-3	2923	238.7	91.0	0.375

References

SKB's (Svensk Kärnbränslehantering AB) publications can be found at www.skb.com/publications.

ASTM, 1996. ASTM D3967-95a, Standard test method for splitting tensile strength of intact rock core specimens, ASTM International, West Conshohocken, PA, USA.

ASTM, 2001. ASTM 4543-01, Standard practice for preparing rock core specimens and determining dimensional and shape tolerance, ASTM International, West Conshohocken, PA, USA.

CEN, 2008. EN 13755:2008. Natural stone test methods – Determination of water absorption at atmospheric pressure, CEN.

Eberhardt E, Stead D, Stimpson B, Read R S, 1998. Identifying crack initiation and propagation thresholds in brittle rock. Can. Geotech. J. 35, pp. 222–233.

Ghazvinian E, Diederichs M, Martin D, Christiansson R, Hakala M, Gorski B, Perras M, Jacobsson L, 2012. Prediction thresholds for crack initiation and propagation in crystalline rocks. ISRM Commission on Spall Prediction Report on Testing Procedures, ISRM.

Gustafsson S E, 1991. Transient plane source techniques for thermal conductivity and thermal diffusivity measurements of solid materials. Rev. Sci. Instrum. 62 (3), March 1991, American Institute of Physics.

ISO, 2015. ISO 22007-2:2015, Plastics – Determination of thermal conductivity and thermal diffusivity – Part 2: Transient plane heat source (hot disc) method, International Organization for Standardization.

ISRM, 1979. Suggested Method for Determining Water Content, Porosity, Density, Absorption and Related Properties and Swelling and Slake-durability Index Properties. Int. J. Rock. Mech. Min. Sci. and Geomech. Abstr, 16(2), pp. 141–156.

ISRM, 1999. Draft ISRM suggested method for the complete stress-strain curve for intact rock in uniaxial compression. Int. J. Rock. Mech. Min. Sci. 36(3), pp. 279–289.

Jacobsson L, Sandström J, Flansbjer M, Sjögren T, Brander L, 2016. ONKALO POSE Experiment – Laboratory Determination of Density, Porosity and Mechanical Anisotropy of Gneiss and Granite, Posiva Working Report 2016-31, Posiva OY Finland.

Martin C D, Chandler N A, 1994. The progressive fracture of Lac du Bonnet granite. Int. J. Rock. Mech. Min. Sci. and Geomech. Abstr. 31(6), pp. 643–659.

Mathworks, 2014. MATLAB Release 2014b, The MathWorks, Inc., Natick, Massachusetts, USA.

Stråhle A, 2001. Definition och beskrivning av parametrar för geologisk, geofysisk och bergmekanisk kartering av berg, SKB-R-01-19. Svensk kärnbränslehantering AB. In Swedish.

Appendix 1

The following equations describe the calculation of radial strains when using a circumferential deformation device, see Figure A1-1.

$\varepsilon_r = \frac{\Delta C}{C_i}$

where

$C_i = 2\pi R_i$ = initial specimen circumference

ΔC = initial specimen circumference = $\frac{\pi \Delta X}{\sin(\theta_i/2)+(\pi-\theta_i/2)\cos(\theta_i/2)}$

and

ΔX = change in LVDT reading = $X_i - X_f$

(X_i = initial chain gap; X_f = current chain gap)

θ_i = initial chord angle = $2\pi - \frac{L_c}{R_i+r}$

L_c = chain length (measured from center of one end roller to center of the other end roller)

r = roller radius

R_i = initial specimen radius

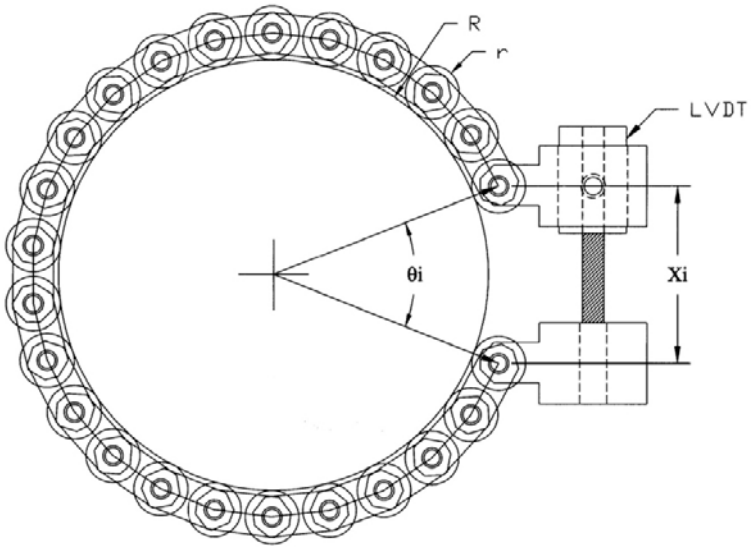

Figure A1-1. *Chain for radial deformation measurement.*

Appendix 2

This Appendix contains results showing the unprocessed data and values on the computed system stiffness K_{system} that was used for the data processing, cf. Section 5.5.2. In addition graphs showing the volumetric strain ε_{vol} versus the axial strain ε_a and the actual radial strain rate $d\varepsilon_r/dt$ versus time are also displayed.

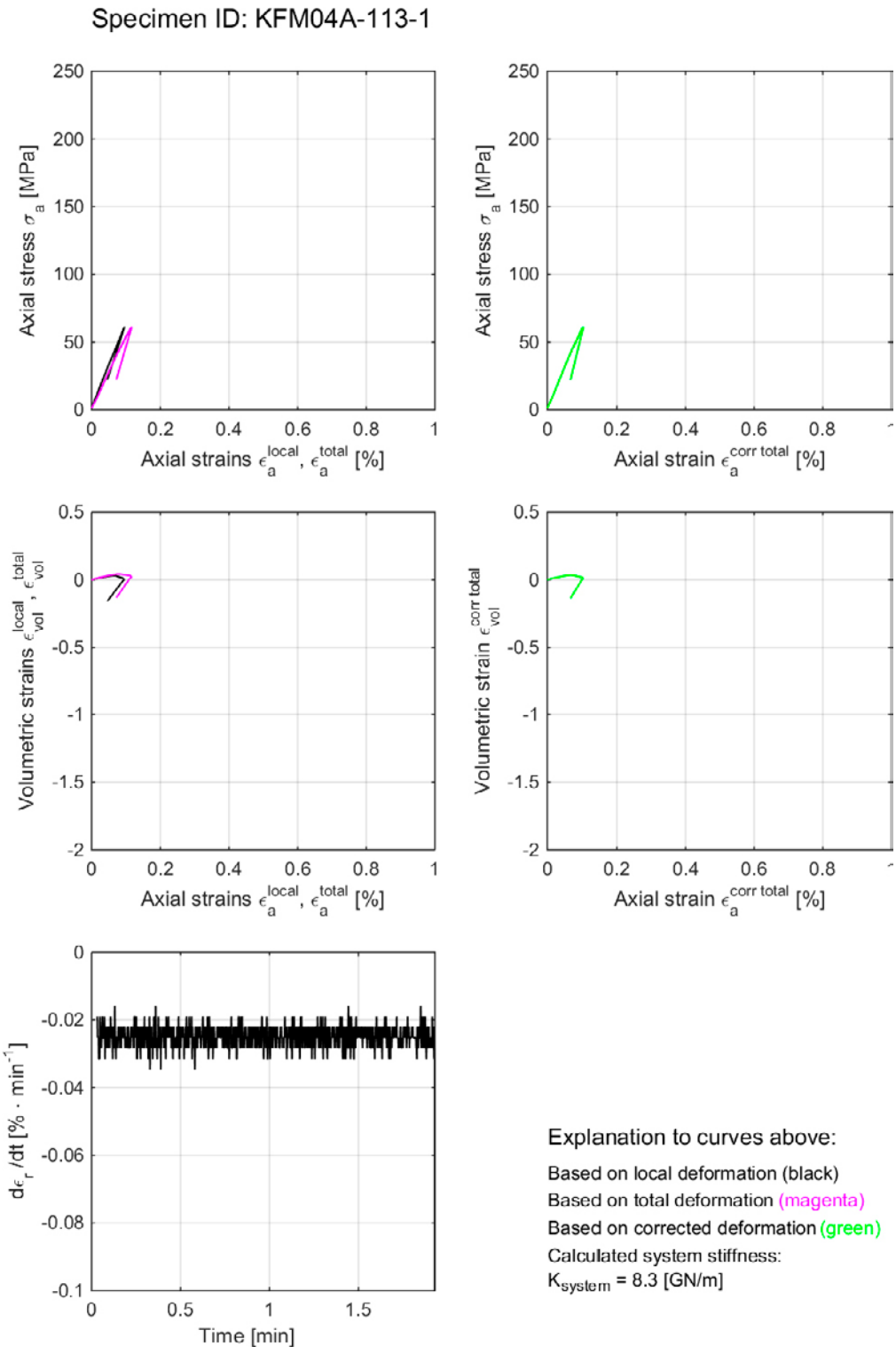

Specimen ID: KFM04A-113-2

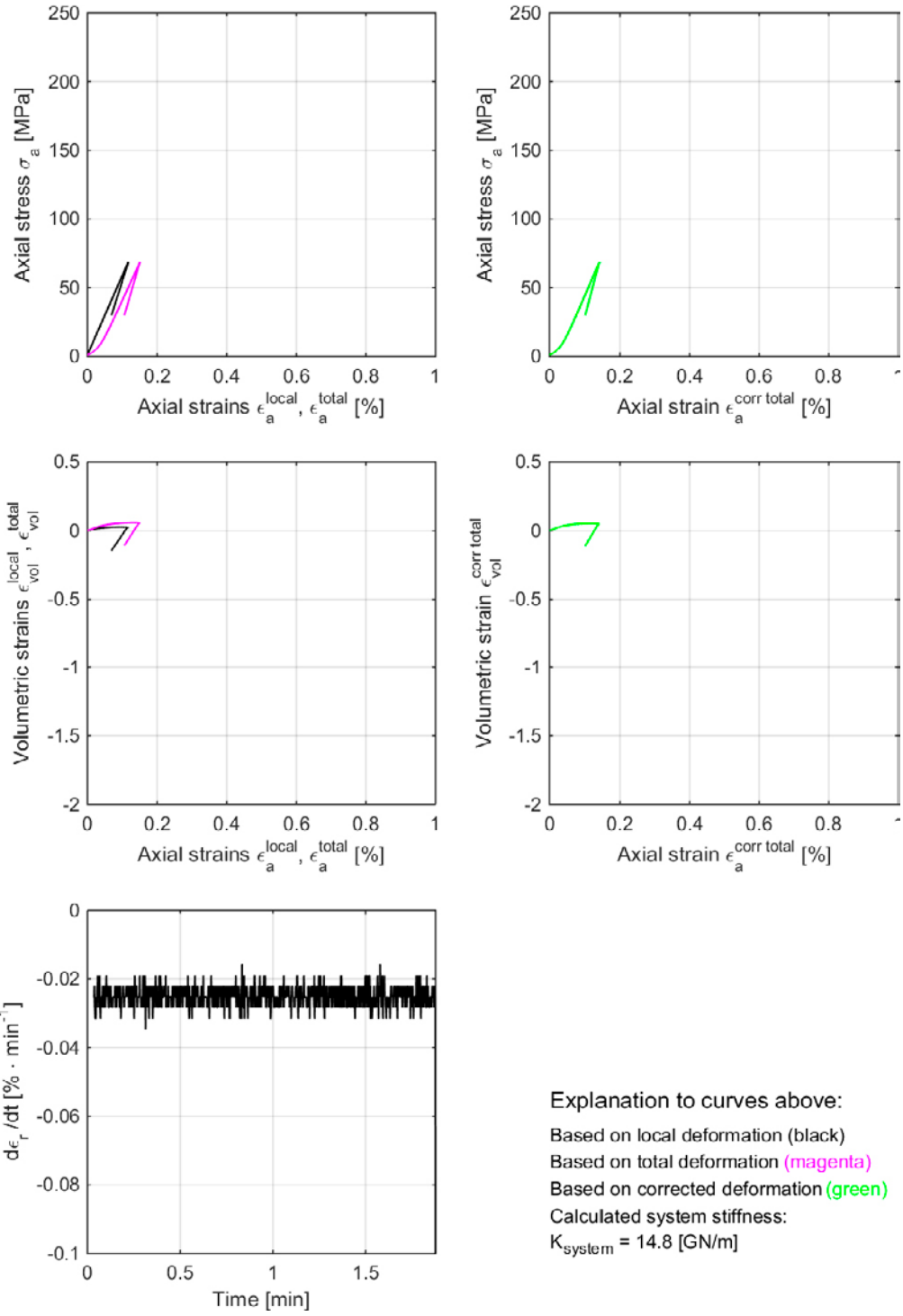

Explanation to curves above:

Based on local deformation (black)
Based on total deformation (magenta)
Based on corrected deformation (green)
Calculated system stiffness:
K_{system} = 14.8 [GN/m]

Specimen ID: KFM24-113-3

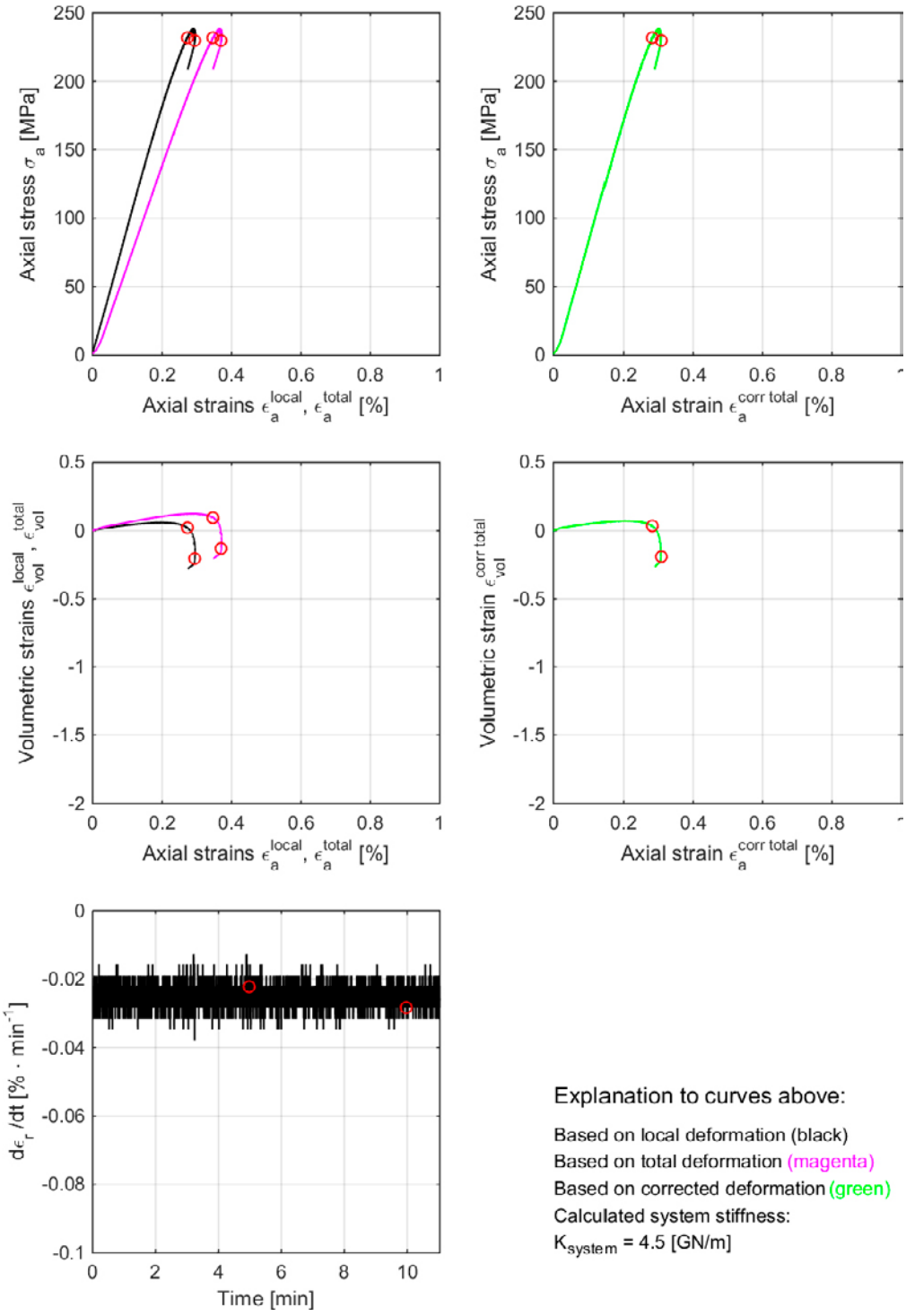

Explanation to curves above:

Based on local deformation (black)
Based on total deformation (magenta)
Based on corrected deformation (green)
Calculated system stiffness:
K_{system} = 4.5 [GN/m]

Arkitektkopia AB, Bromma, 2019

SKB is responsible for managing spent nuclear fuel and radioactive waste produced by the Swedish nuclear power plants such that man and the environment are protected in the near and distant future.

skb.se